

A Spatial Modeling Approach for Linguistic Object Data: Analysing dialect sound variations across Great Britain

Shahin Tavakoli, Davide Pigoli, John A.D. Aston*
Statistical Laboratory, University of Cambridge
and
John S. Coleman
Phonetics Laboratory, University of Oxford

May 25, 2022

Abstract

Dialect variation is of considerable interest in linguistics and other social sciences. However, traditionally it has been studied using proxies (transcriptions) rather than acoustic recordings directly. We introduce novel statistical techniques to analyse geolocalised speech recordings and to explore the spatial variation of pronunciations continuously over the region of interest, as opposed to traditional isoglosses, which provide a discrete partition of the region. Data of this type require an explicit modeling of the variation in the mean and the covariance. Usual Euclidean metrics are not appropriate, and we therefore introduce the concept of d -covariance, which allows consistent estimation both in space and at individual locations. We then propose spatial smoothing for these objects which accounts for the possibly non convex geometry of the domain of interest. We apply the proposed method to data from the spoken part of the British National Corpus, deposited at the British Library, London, and we produce maps of the dialect variation over Great Britain. In addition, the methods allow for acoustic reconstruction across the domain of interest, allowing researchers to listen to the statistical analysis.

Keywords: Functional data analysis, acoustic linguistics data, object data analysis, non-parametric smoothing, covariance matrices.

*The authors gratefully acknowledge support from EPSRC grant EP/K021672/2

1 Introduction

A better understanding of local dialect variation is of interest both from the point of view of linguistics (how languages evolved in the past, how they became differentiated and how they will develop in the future) and from that of social sciences and demography, the way language is used being both a result of social affiliations and a tool to shape group identification. Dialect variations have long been studied in sociolinguistics by considering textual differences between phonetic transcriptions of the words (see, e.g., Kretschmar 1996, Nerbonne & Kretschmar 2003, Nerbonne et al. 2011, and references therein). This focus on written forms reflects a general normative approach towards languages: for cultural and historical reasons, the way we think about them is focused on the written expression of the words, even when thinking of their pronunciations. However, this is more a social artifact than a reality in the population, as there is great variation even within a single region with a claimed “homogeneous” dialect. Indeed, the analysis of speech data highlights that the definition of language is an abstraction that simplifies the reality of speech variability and neglects the continuous geographical spread of spoken varieties, although this does not exclude the presence of some clearly defined boundaries.

In this paper, we develop techniques that explicitly complement this text-based approach; we define methodology not for written or transcription based analysis, but rather by treating the acoustic data directly, by considering sounds as data objects (see Wang et al. 2007, for a definition of data objects). This allows the examination of all forms of variation, including those within groups usually deemed to be homogeneous. To achieve this requires the development of spatially varying statistical models for object data which take into account both the underlying geography, but also the statistical properties of the data (in this case the fact that part of the model requires estimation of quantities which lie on a manifold). This leads to the definition of a new concept of covariance which is statistically consistent over space even under Fréchet type estimation.

We are particularly interested in using information from speech recordings to model the smooth variation of speech characteristics over a geographical region. Since recordings are obtained only in a discrete set of locations, the first step will be the development of a non-parametric smoothing procedure to infer speech characteristics (and plausible speech reconstruction) on the continuous map. Having available replicates from different speakers at each location, we are able to model both the mean and the covariance structure of the speech process at that single location, the latter being highlighted in recent studies (see Aston et al. 2010, Hadjipantelis et al. 2012) as an important feature for language characterization. The model we use to smooth the speech process over the whole geographical region of interest is described in Section 3, with the model based on the concept of using data specific metrics in the analysis.

From a statistical point of view, we develop the concept of spatial object data analysis, and, in particular, the use of d -covariances, that is, covariances that are estimated under a different metric to the usual Euclidean (L^2) one. It has been seen in a variety of applications, particularly diffusion tensor imaging, that even when the use of Euclidean distance is appropriate (and in the case of defining geodesics it may well not be so), it is often sub-optimal in terms of interpretability (see for example Dryden et al. 2009). This is particularly important for the case of spatial smoothing with replicates, as use of the implied Euclidean metric (as is

the case for the sample covariance) is not consistent with a spatially smoothed version under another metric, while the Euclidean metric is not valid with general smoothing techniques for positive definite covariances. Thus a new type of covariance will be developed which is statistically consistent. The analysis of the covariance structure is made possible by the presence of replicates of the same sound, uttered by different speakers, in each geographical location. This is an uncommon setting for spatial data analysis which is usually focused on problems where replicates are not available but second-order stationarity can be assumed. The latter is also the setting where most of the recent work on spatial statistics for object data have been developed (see, e.g., Delicado et al. 2010, Gromenko et al. 2012, Menafoglio & Petris 2016). In this work, the need to model the spatial variation of the covariance structure of the speech process led us to choose a non-parametric regression approach to estimate both the mean and the d -covariance of the speech process, in the line of the methods developed for interpolation and smoothing of positive definite matrices (Dryden et al. 2009, Yuan et al. 2012) and for surface smoothing over complex domains (Wood et al. 2008, Sangalli et al. 2013).

We also develop a set of tools to communicate relevant information to linguists. First, we generate colour maps that reflect speech variation in the spirit of isogloss maps (see, e.g., Francis 1959, Upton & Widdowson 2013) but with continuous variation (as opposed to hard boundaries) and using information from speech recordings (as opposed to achieving this via phonetic transcriptions). Moreover, our method allows the resynthesis of a plausible pronunciation for any point in the considered geographical region. We include as supplementary material a few examples of these reconstructed pronunciations for the sound data set described in Section 2.

The paper proceeds as follows. In Section 2, the principles behind using acoustic recordings as the intrinsic data objects, as well as the data set itself, are introduced. Section 3 develops both the concept of d -covariance and the model for spatial data objects based on the d -covariance formulation. Section 4 applies the modeling framework to the British National Corpus data. This data set is a large corpus of acoustic recordings of British English across Great Britain, making it ideal for the comparison of dialects and accents. Finally, Section 5 is a discussion of the work and both its linguistic and statistical relevance. Some technical results concerning d -covariances and the model, as well as additional informations about the preprocessing are given in the appendix. The data, associated R code (R Core Team 2016) to replicate the analysis, supplementary figures and details on the data preprocessing are available as supplementary materials.

2 Sounds As Data Objects

In linguistics, there has recently been a considerable interest in assessing information coming directly from speech recordings (Lehmann 2004, The Functional Phylogenies Group 2012, Pigoli et al. 2014, Hadjipantelis et al. 2015, Coleman et al. 2015) in addition to textual evidence and phonetic transcriptions. While we develop new methodologies that can be applied to a variety of languages and geographical regions, we consider, in particular, the variation of the English language in the United Kingdom. British English is well known to contain a large number of regional dialects, which can have considerable differences between them.

Dialect variation is investigated by analysing the spoken part of the British National Corpus (BNC) deposited at the British Library. The digital versions of these recordings are now made available by the Phonetics Laboratory of the University of Oxford (Coleman et al. 2012). These sound data (rather than their phonetic transcriptions) will be directly used to explore British dialects. In particular, for the statistical analysis of speech tokens, it is first necessary to represent sounds in a time-frequency domain and align them in time to account for individual variation in speaking rate. We choose here a Mel Frequency Cepstral Coefficients representation for the speech tokens because of its good performance for speech resynthesis (which will be the final output of our analysis), and because it provides a principled lower dimensional representation of the speech tokens. We now give a more detailed description of the underlying data and their mathematical representation.

2.1 Sound Waves, Spectrograms, and Mel-Frequency Cepstral Coefficients

A one-channel monophonic sound can be represented by a time series $(s(t) : t = 1, \dots, T)$, where $s(t)$ represents the recording of the air pressure at time t as captured by the microphone. As such, a sound is the variation of air pressure over time. For $t \leq 0$ or $t > T$, we let $s(t) = 0$. We can therefore assume that $s(t)$ is well defined for $t \in \mathbb{Z}$. An example of sound wave is given in Figure 1.

The spectrogram of a sound $(s(t))_{t=1,\dots,T}$ is a two-dimensional representation $\text{Spec}(s)(t, \omega)$ of the sound, where $\text{Spec}(s)(t', \cdot)$ represents the modulus of the discrete Fourier transform of $s(t)$ in a neighborhood of t' . Mathematically, if $W(x), x \in \mathbb{R}$ in a window function with support $[-1, 1]$, then for any positive integer $M, w_M(t) = W(2t/M), t \in \mathbb{Z}$ is a window of width M , and

$$\text{Spec}(s)(t, \omega) = \left| \sum_{u=1}^T s(t-u)w_M(u) \exp(-i\omega u) \right|, \quad t = 1, \dots, T, \omega \in [0, 2\pi].$$

The function $u \mapsto s(t-u)w_M(u)$ is a windowed version of s around t . For computational efficiency, the spectrogram is computed at the Fourier frequencies $\omega \in \{2\pi k/N\}$, where $N \geq T$ is highly composite (usually a power of 2), using the fast Fourier transform (FFT; Cooley & Tukey 1965). The window width M is typically chosen to correspond to a segment of length ranging from 5 to 20 milliseconds ($M = 80$ or 320 at 16Khz). From now on, we shall call the spectrogram of s the $T \times N$ matrix with entries $\text{Spec}(s)(t, \omega_k), t = 1, \dots, T, \omega_k = 2\pi k/N, k = 0, \dots, N-1$.

A low dimensional time-frequency representation of the sound wave, often used in speech recognition and speech synthesis, are the *Mel-frequency cepstral coefficients*, or *MFCC*. The computation of the MFCC is done in two steps. First, the *Mel spectrogram*, a filtered version of the spectrogram is computed,

$$\text{MelSpec}(s)(t, f) = \sum_{k=0}^{N-1} \text{Spec}(s)(t, 2\pi k/N) b_{f,k}, \quad f = 0, \dots, F,$$

where $(b_{f,k})_{k=0,\dots,N-1}, f = 0, \dots, F$ is the so-called Mel-scale filter bank (an example of a Mel-scale filter bank is given in Gold et al. 2011) with F filters, which is believed to mimic the

human ear auditory system. Then, the MFCC corresponds to the first $M \leq F$ coefficients of the inverse Fourier transform of the Mel spectrogram:

$$\text{MFCC}_s(t, m) = \frac{1}{F} \sum_{f=0}^F \text{MelSpec}(s)(t, f) \exp[i(2\pi(m-1)/(F+1))f], \quad m = 1, \dots, M.$$

An additional reason to prefer MFCC over spectrograms is that each coefficient is associated to a frequency band, and therefore the MFCCs are more robust to small misalignments in frequency when comparing multiple speakers or sounds. Since the MFCCs are assumed to be smooth in t , we shall from now on assume that $t \in [0, 1]$, where it is implicitly assumed that the integer t are replaced by t/T and interpolated. An example of MFCC is given in Figure 1.

Note that there exist many modifications and variations of this definition of MFCC in the literature, as authors seek improvements in the performance of implemented speech recognition or parametric speech synthesis systems. Since one of the goals of this paper is the resynthesis of sounds after inference, we shall use the definition and computational implementation of the MFCC proposed in Erro et al. (2011, 2014) as it yields high-quality, natural sounding resynthesised speech. However, the underlying principles are the same. For simplicity, we will refer in the following to this modified version as MFCC.

2.2 The British National Corpus

The raw data consist of the audio British National Corpus (BNC) recordings (131 GB of data, 16 Bit 16 kHz one-channel .wav files, roughly 1100 hours of recording, publicly available at <http://www.phon.ox.ac.uk/AudioBNC>). These are mainly recordings of natural speech in typically noisy environments, with low recording amplitude (signal-to-noise ratio). Segmentation information about the words pronounced in the audio files were also provided (in TextGrid format), with the XML edition of the BNC (4.4 GB of files) containing transcriptions of the words spoken in the audio BNC recordings, along with contextual information (anonymized speaker identification, information about the speakers, location of the recording).

For the purposes of the current paper, we restricted ourselves to the analysis of sounds of the vowel “a” present in the following list of words:

$$\text{class, glass, grass, past, last, brass, blast, ask, cast, fast, pass.} \quad (2.1)$$

The vowels in these words are pronounced in the same (geographically consistent) way and therefore we can consider them as the replicates of the same sound. We denote this as the “class” dataset. In Great Britain, this vowel is considered prototypical of the distinction between northern and southern accents: in the Midlands, North and South-West these words have a short, open front vowel [a] as in “pat”, whereas in the South and South-East they have a long back vowel [ɑ] (“aah”), similar to the vowel in “part”. The purpose of our work is the spatial analysis of sounds, and as such we needed to assign to each recorded sounds to the geographical location of the speaker’s origin. We therefore removed sounds of speakers with missing or vague location information, and sounds corresponding to speakers who where

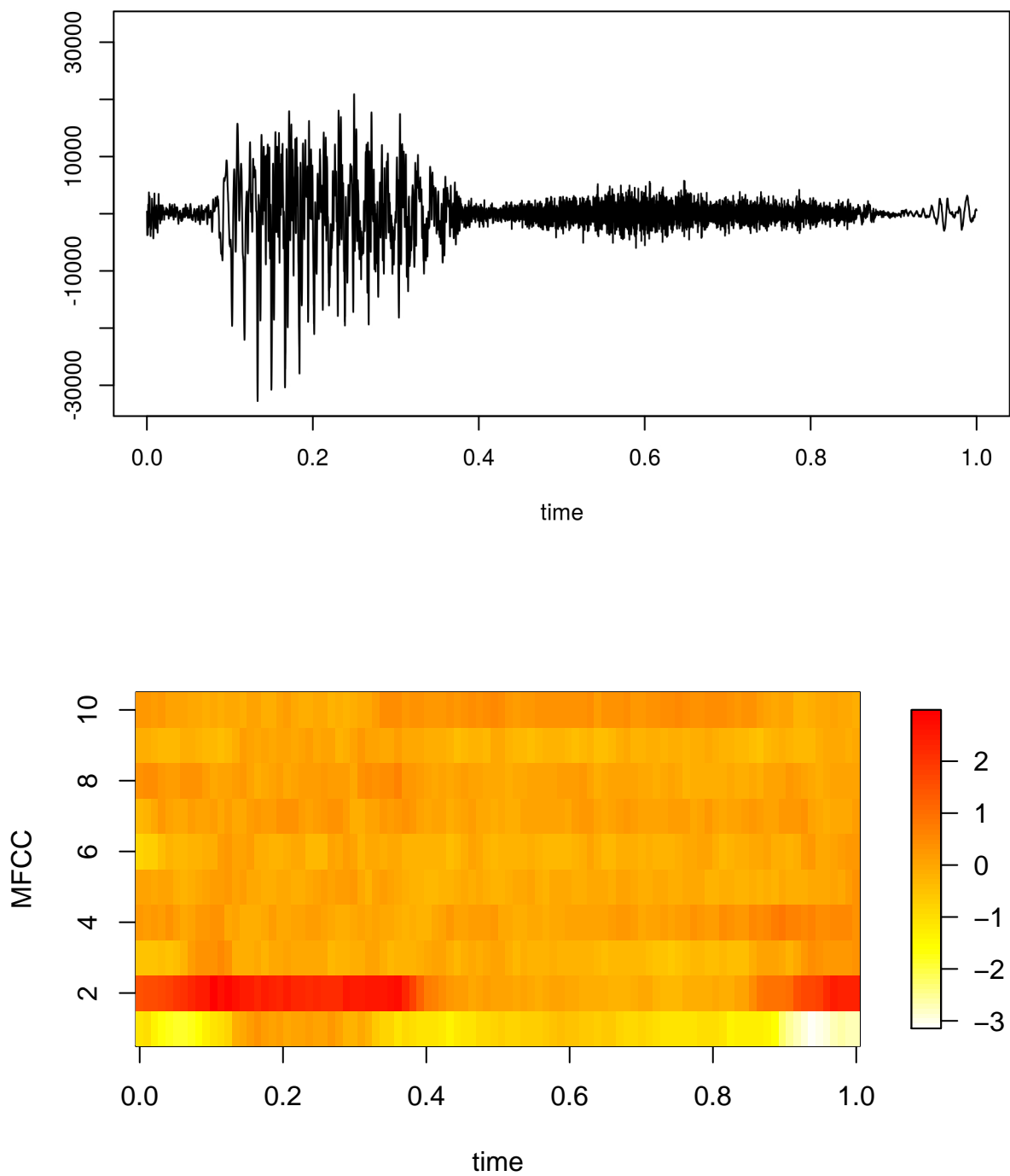


Figure 1: Top figure: sound wave $s(t)$ of the word 'last'. Bottom figure: corresponding $\text{MFCC}_s(t, m)$. Both time scales have been normalized to $[0, 1]$.

trained to speak in a specified fashion (such as TV or radio presenters). For each speaker, we then used the corresponding recording location (the variable `placenamecleaned`) as a surrogate for the speaker’s origin, provided this was unique. If there were multiple recording locations for a given speaker, the location corresponding to the `locale` variable “home” or “at home” was taken as the location of origin. If no such location existed, the sounds corresponding to the speaker were discarded. It should be noted that although we assume the speaker’s accent to be representative of his recording location, there is unfortunately no data about the origin of the speakers to corroborate this assumption.

After this process, we obtained 4816 sound tokens from 110 distinct geographical locations in Great Britain, with 1993 distinct speaker-vowel (from distinct word) combinations. About 46% of the speaker-vowel combinations appear more than once, 61 speaker-vowel combinations appear at least 10 times, and there is a speaker-vowel combination that is repeated 34 times in the dataset. While the model we will use in Section 3 could be extended to a random effects type setup, to account for speaker repetition, we prefer to concentrate on the simpler model to aid understanding, particularly as most speaker vowel combinations only appear once.

These vowel sounds were then transformed into MFCCs, with $M = 10$. For each word w in our list of words (C.1), we aligned the MFCCs of sounds corresponding to w by registering their first coefficient (which corresponds to relative volume) using the Fisher-Rao metric (R package `fdasrvf`; see Srivastava et al. 2011, Tucker et al. 2013, Wu & Srivastava 2014) and then extracted the segment associated to the vowel for each word, and linearly rescaled its time to the unit interval $[0, 1]$. Furthermore, we centered the first cepstral coefficients of all the data to remove differences in recording volume. For further information concerning the preprocessing and alignment, see the Appendix.

We note that the duration of the vowel sounds is lost in the preprocessing step, and as such, we present a spatial map of the vowel durations in the Appendix (Figure A5). Indeed, the vowel duration is a one scalar summary of the sound of the vowel, which although useful does not capture considerable additional qualitative information contained in the vowel sound MFCCs, even after time alignment.

3 Model and Estimation

As mentioned earlier, previous works have identified the covariance structure between frequencies as an important feature of the speech process that characterises languages (Aston et al. 2010, Hadjipantelis et al. 2012, Pigoli et al. 2014, Hadjipantelis et al. 2015). We therefore have good reasons to expect the covariance between MFCCs—which are related to the energy in each frequency band—to be associated with dialect characteristics, and we want to allow for it to vary geographically. The investigation of the best metric for interpolation or extrapolation of covariance matrices or operators has recently generated much work (Arsigny et al. 2007, Dryden et al. 2009, Yuan et al. 2012, Carmichael et al. 2013). The use of a metric different from the Euclidean metric in the analysis leads to the formulation of a more general concept of co-variability: the d -covariance. In the following, we explain why we need to introduce this new concept and the role it plays in the definition of the model for speech variation presented in Section 3.2.

3.1 d -covariances

Interpolation of covariance matrices under the usual Euclidean metric, although yielding valid covariances, suffers from artifacts, such as swelling (e.g. Arsigny et al. 2006). Extrapolation of covariances under the Euclidean metric, on the other hand, is not even guaranteed to give valid covariances. For this reason, several other metrics on the spaces of symmetric positive semi-definite matrices have been studied, and have been shown to be useful for interpolation or extrapolation of covariances. For instance, the Euclidean average $\overline{C} = n^{-1} \sum_{i=1}^n C_i$ of covariance matrices C_1, \dots, C_n can be reformulated as the solution to the variational problem

$$\min_{\Omega} \sum_{i=1}^n d_E^2(\Omega, C_i),$$

where d_E denotes the Euclidean distance. In other words, \overline{C} is the Fréchet mean of C_1, \dots, C_n under d_E . Therefore the average of covariances C_1, \dots, C_n under another metric d can be defined as their Fréchet mean under d .

While covariance interpolation or extrapolation under various metrics is useful (for example in the case of spatial smoothing; see e.g. Yuan et al. 2012), it is only valid when treating the covariances C_i as the observation units. However, the covariances C_i are estimators of unknown true covariances, and have therefore an intrinsic estimation error. Since the true covariance of a random vector $X \in \mathbb{R}^p$ can be defined as the solution of the variational problem

$$\min_{\Omega} \mathbb{E} d_E^2(\Omega, (X - \mu)(X - \mu)^\top),$$

the sample covariance can be viewed as an analogue sample-based variational problem *based on the Euclidean metric d_E* . When using a metric different than d_E for spatial smoothing of sample covariances, a consistency problem arises due to the two different metrics used in the variational problem and the smoothing problem, and the resulting estimator is biased. A one-dimensional example illustrating this is given in Section F of the Appendix.

For this reason, we introduce the concept of d -covariance that stems from recent developments on the inference for covariance operators (see Arsigny et al. 2006, Dryden et al. 2009, Kraus & Panaretos 2012, Pigoli et al. 2014, Petersen & Müller 2016a), where d is a metric on the space of $p \times p$ symmetric positive semi-definite matrices \mathcal{S}_p that is used for the spatial smoothing. The d -covariance of a random vector $X \in \mathbb{R}^p$ is denoted $\text{cov}_d(X)$, and defined by

$$\text{cov}_d(X) = \underset{\Omega \in \mathcal{S}_p}{\text{argmin}} \mathbb{E} d^2((X - \mu)(X - \mu)^\top, \Omega),$$

where $\mu = \mathbb{E} X$, and provided the right-hand side is well defined.

In this paper, we shall use the square-root metric d_S on the space of symmetric positive semi-definite matrices, defined by $d_S(B, C) = \left\| \sqrt{B} - \sqrt{C} \right\|$, where \sqrt{B} , also written $B^{1/2}$, is the unique square root of B (meaning that it is the unique matrix D that satisfies $DD = B$; see Appendix A), and $\|\cdot\|$ is the Frobenius norm. As can be seen in the one-dimensional example given in Section F of the Appendix, using the same metric d_S for both the definition of the co-variation and the spatial smoothing yields an estimator that is less biased than the one obtained by spatial smoothing of the usual (Euclidean) covariance with d_S . Let

$|\cdot|$ denote the Euclidean norm on \mathbb{R}^p , i.e. $|x| = \sqrt{x^\top x}$. The following Proposition gives an explicit formula for the d_S -covariance.

Proposition 3.1. *Let $X \in \mathbb{R}^p$ be random element with $\mathbb{E}|X| < \infty$ and mean $\mu = \mathbb{E}X$. Then $\text{cov}_{d_S}(X) = \mathbb{E} \left[\sqrt{(X - \mu)(X - \mu)^\top} \right]^2$.*

Notice in particular that we do not need second moments for the d_S -covariance to exist, which is due to the fact that $\left\| \sqrt{XX^\top} \right\| = |X|$. Since there is an explicit formula for the square-root of symmetric positive semi-definite matrices of rank one, namely $\sqrt{xx^\top} = xx^\top/|x|$, for $x \in \mathbb{R}^p, x \neq 0$, we can rewrite the d_S -covariance of X as

$$\text{cov}_{d_S}(X) = \mathbb{E} \left[\frac{(X - \mu)(X - \mu)^\top}{|X - \mu|} \right]^2, \quad (3.1)$$

where the expression inside the expectation is understood to be equal to zero if $X = \mu$. The denominator in (3.1) reveals that the square-root of the d_S -covariance can be viewed as a regularized version of the usual covariance. Furthermore, it also reveals that unlike the Euclidean covariance, the d_S -covariance does not behave in the usual way under linear transformations: $\text{cov}_{d_S}(AX) \neq A \text{cov}_{d_S}(X) A^\top$ for general linear transformations A . However, if we introduce the new families of square-root semi-metrics $d_{S,A}(C, D) = \left\| \sqrt{ACA^\top} - \sqrt{ADA^\top} \right\|$, where C, D are $p \times p$ symmetric positive semi-definite matrices and A is a $n \times p$ matrix, we have the following result, proved in Appendix B.

Proposition 3.2. *Let A be a $n \times p$ matrix, and $X \in \mathbb{R}^p$ be a random element with $\mathbb{E}|X| < \infty$. Then $\text{cov}_{d_S}(AX) = A \text{cov}_{d_{S,A}}(X) A^\top$.*

This means that the d_S -covariance of a linear transformation of X is given by a transformation of the d -covariance of X under a metric related to the linear transformation. In particular, the entries of a d_S -covariance do not correspond to the d_S -covariance of corresponding entries of the random vector. This is analogous to partial correlation.

3.2 A model for spatially varying speech object data

We are now ready to define the model for speech variation for the analysis of dialect data. We wish to have a model which can spatially vary both in terms of a mean function but also in terms of covariance, as we will have replicates at individual spatial locations. We therefore assume the following model:

$$Y_{lj}(t) = m(X_l, t) + \varepsilon_{lj}(t), \quad l = 1, \dots, L; j = 1, \dots, n_l, \quad (3.2)$$

where $Y_{lj}(t) \in \mathbb{R}^p$ is the vector of the first p Mel-frequency cepstral coefficient (MFCC) at time $t \in [0, 1]$ of the recording lj , X_l corresponds to the spatial location of the observations $Y_{lj}, j = 1, \dots, n_l$, recorded in latitude/longitude coordinates, i.e. $X_l \in \mathcal{E}$, where $\mathcal{E} \subset (-90, 90] \times (-180, 180]$ is the spatial domain, and will denote Great Britain in the application of Section 4. The *spatial MFCC* is the function $x \mapsto m(x, \cdot) \in L^2([0, 1], \mathbb{R}^p)$, mapping a spatial location $x \in \mathcal{E}$ to its corresponding mean MFCC.

The term $\varepsilon_{lj} \in L^2([0, 1], \mathbb{R}^p)$ is an error term. We assume that for each $l = 1, \dots, L$, $\varepsilon_{lj} \stackrel{\text{iid}}{\sim} \varepsilon(X_l)$, $j = 1, \dots, n_l$, and that the ε_{lj} s are all independent. Indeed, this is a valid assumption since we have replicates for each location X_l , and a scatterplot of the pairwise distances between the errors against their geographical distances does not reveal any spatial dependence (see Figure A6 of the Appendix). The process $\varepsilon(\cdot) : \mathcal{E} \rightarrow L^2([0, 1], \mathbb{R}^p)$ is assumed to have mean zero, $\mathbb{E}\varepsilon = 0$, and we denote its d_S -covariance by $\Omega(x, t) = \text{cov}_{d_S}(\varepsilon(x, t))$, where we write $\varepsilon(x, t)$ for $\varepsilon(x)(t)$. This implies in particular that $\text{cov}_{d_S}(Y_{lj}(t)) = \Omega(X_l, t)$. While traditionally $\Omega(X_l, t)$ would be defined as the covariance matrix of Y_{lj} , by assuming that $\mathbb{E}\varepsilon_{lj}(t) = 0$ for all t and $\mathbb{E}[\varepsilon(t)\varepsilon(t)^\top]$ is the identity, we define here $\Omega(X_l, t)$ to be the d_S -covariance of Y_{lj} , where d_S is the square-root metric, because we shall be smoothing spatially using the metric d_S . Recalling that $\mathcal{S}_p \subset \mathbb{R}^{p \times p}$ is the space of symmetric positive semi-definite $p \times p$ real matrices, the function $x \mapsto \Omega(x, \cdot) \in L^2([0, 1], \mathcal{S}_p)$, maps a spatial location $x \in \mathcal{E}$ to a time-varying symmetric positive semi-definite matrix at that location.

Given the observations $\{Y_{lj}(t), X_l\}$, we want to estimate a smooth field $\hat{m}(x, t)$ for the mean of the speech process, and a smooth field $\hat{\Omega}(x, t)$ for the (time-dependent) d_S -covariance between MFCCs coefficients.

3.3 Estimation of the mean MFCCs field

In this section, we will be dealing with the estimation of the mean MFCC field m , and therefore the natural metric in this case to consider is the Euclidean (L^2) distance. However, when we consider the geographical distance, the natural metric is the geodesic distance, which we will approximate by graph distance $d_g(\cdot, \cdot)$ on a constructed triangular mesh over the region of interest.

We propose to fit the mean MFCC field using a local constant estimator which minimizes a weighted mean square fit criterion. Let $K : \mathbb{R} \rightarrow [0, \infty)$ denote a continuous and bounded density function, and let $K_h(s) = K(s/h)/h^2$. At the location x , the estimate of the mean MFCC is $\hat{m}(x) \in L^2([0, 1], \mathbb{R}^p)$ which minimizes

$$\sum_{l=1}^L \sum_{j=1}^{n_l} K_h(d_g(x, X_l)) \frac{\|Y_{lj} - \hat{m}(x)\|^2}{\hat{\sigma}^2(X_l)}, \quad (3.3)$$

where $\|\cdot\|$ is the usual norm in $L^2([0, 1], \mathbb{R}^p)$, i.e. $\|f\|^2 = \int_0^1 |f(t)|^2 dt$ for $f \in L^2([0, 1], \mathbb{R}^p)$, and $d_g(x, X_l)$ is the distance on the map between x and X_l . The denominator is a normalizing factor that compensates for possible heteroscedasticity in the MFCC field using the total variability of the residuals, $\hat{\sigma}^2(X_l) = n_l^{-1} \sum_{j=1}^{n_l} \|Y_{lj} - \bar{Y}_l\|^2$, where $\bar{Y}_l = n_l^{-1} \sum_{j=1}^{n_l} Y_{lj}$. The minimizer of the fit criterion (3.3) is a Nadaraya–Watson type estimator, given by convex combination of the average MFCCs at each location, i.e.

$$\hat{m}(x) = \sum_{l=1}^L w_l(x) \bar{Y}_l, \quad (3.4)$$

where

$$w_l(x) = \tilde{w}_l(x) / \sum_{l'=1}^L \tilde{w}_{l'}(x) \quad \& \quad \tilde{w}_l(x) = n_l \cdot K_h(d_g(x, X_l)) / \hat{\sigma}^2(X_l)$$

Possible strategies for the choice of the bandwidth h are discussed in Section 4.1. It may be argued that using a higher order local polynomial estimator in place of (3.3) can reduce the bias of the estimator, and there exists methods to perform local linear smoothing when only pairwise distances between the covariates are available (Baíllo & Grané 2009, Boj et al. 2010, 2016). We leave this extension as a future avenue of research.

3.4 d_S -Covariance Field Estimation

In this section, we extend the kernel smoother to estimate the smooth d_S -covariance field Ω . The natural metric to be used for the smoothing in this case is the square root metric d_S as this indeed avoids inconsistencies between estimation of the d_S -covariance in the observed locations and estimation of the spatially smooth field, as we show in Section 3.5. Moreover, the square root metric is well-defined for singular matrices, a property that will be needed for the application to the BNC data in Section 4. Indeed, locations with small number of observations are expected to have d_S -covariance between MFCCs that are not full rank. We also propose to use a locally constant estimator of the covariance field to allow for the non-convex domain, as discussed in the previous section.

At the point x , the estimated covariance $\hat{\Omega}(x, \cdot) \in L^2([0, 1], \mathcal{S}_p)$ is the minimizer of the following fit criterion:

$$\sum_{l=1}^L K_h(d_g(x, X_l)) \int_0^1 d_S^2(\check{\Omega}_l(t), \hat{\Omega}(x, t)) dt, \quad (3.5)$$

where h is a smoothing parameter, and $\check{\Omega}_l \in L^2([0, 1], \mathcal{S}_p)$ is the sample d_S -covariance at location X_l , defined as

$$\begin{aligned} \check{\Omega}_l(t) &= \operatorname{argmin}_{\Omega \in \mathcal{S}_p} \frac{1}{n_l} \sum_{i=1}^{n_l} d_S^2(\Omega, (Y_{li}(t) - \bar{Y}_l(t))(Y_{li}(t) - \bar{Y}_l(t))^T), \quad \text{for each } t \in [0, 1]. \\ &= \left[\frac{1}{n_l} \sum_{i=1}^{n_l} \sqrt{(Y_{li}(t) - \bar{Y}_l(t))(Y_{li}(t) - \bar{Y}_l(t))^T} \right]^2 \end{aligned}$$

It is not difficult to show that the minimizer of (3.5) is given by

$$\hat{\Omega}(x, t) = \left[\sum_{l=1}^L w_l(x) \sqrt{\check{\Omega}_l(t)} \right]^2, \quad (3.6)$$

where

$$w_l(x) = \tilde{w}_l(x) / \sum_{\nu=1}^L \tilde{w}_\nu(x) \quad \& \quad \tilde{w}_l(x) = K_h(d_g(x, X_l)). \quad (3.7)$$

Equation (3.6) reveals that $\hat{\Omega}(x)$ is the square of a Nadaraya–Watson estimator in the square-root space.

3.5 Consistency of Smoothing with the Square Root Distance

In this section, we study the properties of the estimator for the d_S -covariance smooth field $\Omega(x, t)$. This is a non-standard smoothing problem, which poses a few theoretical challenges due to the non-Euclidean metric involved, and to the fact that we want to control the estimation error uniformly in the time index. Moreover, this gives us the opportunity to show how it is possible to account for the use of the geographical distance d_g in the kernel smoothing. The estimator for the mean field $m(x, t)$ uses the Euclidean (L^2) metric and its properties can therefore be studied using similar arguments, in particular using the results in Appendix B.

This first result, proved in Appendix B, shows that under mild assumptions, the sample d_S -covariance is a \sqrt{n} -consistent estimator of the d_S -covariance.

Proposition 3.3. *Let $Y_1, \dots, Y_n \stackrel{\text{iid}}{\sim} Y \in \mathbb{R}^p$ be random vectors with $\mu = \mathbb{E}Y$ and $\mathbb{E}|Y|^2 < \infty$. Let $\bar{Y} = (Y_1 + \dots + Y_n)/n$, and*

$$\check{\Omega} = \left(\frac{1}{n} \sum_{i=1}^n \sqrt{(Y_i - \bar{Y})(Y_i - \bar{Y})^\top} \right)^2,$$

this being the explicit expression for the sample d_S -covariance. Then $d_S(\check{\Omega}, \text{cov}_{d_S}(Y)) \leq \kappa_p \sqrt{\mathbb{E}|Y - \mu|^2/n}$, where κ_p is a constant depending only on the dimension.

In particular, $\check{\Omega} = \text{cov}_{d_S}(Y) + O_{\mathbb{P}}(n^{-1/2})$. We now introduce some conditions used in proving the consistency of the smooth d_S -covariance field.

Condition 3.4.

- (1) *The kernel $K : \mathbb{R} \rightarrow [0, \infty)$ is a continuous probability density, with $\int_0^\infty s^3 K(s) ds < \infty$. Assume also that K is decreasing, i.e. $0 \leq s \leq t \implies K(s) \geq K(t)$.*
- (2) *There exists constants $0 < c_1 < c_2$ such that $c_1|x - y| \leq d_g(x, y) \leq c_2|x - y|$.*

Condition 3.4 (1) is a standard condition on the kernel function, which is in particular satisfied by the Gaussian kernel we use in Section 4. Condition 3.4 (2) states that the graph distance is (metric) equivalent to the Euclidean distance on \mathcal{E} . The following condition on the sampling density is standard.

Condition 3.5. *The density of the observation locations $X_1, \dots, X_L \in \mathcal{E}$, $f : \mathcal{E} \rightarrow \mathbb{R}$ is continuous, and $\sup_{x \in \mathcal{E}} f(x) < \infty$.*

Recall that $\Omega(x, t) = \text{cov}_{d_S}(\varepsilon(x, t))$. We are going to assume the following regularity conditions on the error process ε .

Condition 3.6.

- (1) *$n_l \geq c_0 n$ for all $l = 1, \dots, L$ for some $c_0 > 0$.*

- (2) $\sqrt{\Omega(\cdot, t)} : \mathcal{E} \rightarrow \mathcal{S}_p$ is C^1 (with respect to the Hilbert–Schmidt norm), and
- $$\sup_{x \in \mathcal{E}, t \in [0, 1]} \left| \frac{\partial [\sqrt{\Omega(x, t)}]_{rs}}{\partial x}(x) \right| < \infty, \text{ where } [A]_{rs} \text{ is the } rs\text{-th entry of the matrix } A.$$
- (3) $\sup_{x \in \mathcal{E}, t \in [0, 1]} \mathbb{E} |\varepsilon(x, t)|^2 < \infty.$

Condition 3.6 (1) states that asymptotically, the number of observations per locations is of the same order. Condition 3.6 (2) is a (pointwise in time) smoothness condition on the d_S -covariance field. Condition 3.6 (3) assumes that the second moment of the error field is uniformly bounded. The second moment is needed to establish the rate of convergence, whereas the uniform bound is for the control of the smoothing error uniformly in time.

We can now state the result on the consistency of the smoothed d_S -covariance field, whose proof is in Appendix B.

Theorem 3.7. *Assume model (3.2) with conditions 3.4, 3.5 and 3.6 holds, and $L \rightarrow \infty, h \rightarrow 0, Lh \rightarrow \infty, n \rightarrow \infty$. Then, for any $x \in \mathcal{E}$ in the interior of \mathcal{E} such that $f(x) > 0$, we have*

$$\mathbb{E}_X d_S(\hat{\Omega}(x, t), \Omega(x, t)) = O_{\mathbb{P}}(n^{-1/2}) + O_{\mathbb{P}}\left(\sqrt{h^2 + \frac{1}{nLh^2}}\right),$$

where the stochastic term is uniform in t , and \mathbb{E}_X is the expectation conditional on X_1, \dots, X_L .

The first error term comes from the fact that we are using the sample mean in place of the true mean in the computation of the sample d_S -covariance, while the second error term is a bias plus variance decomposition. Notice that the n in the variance term is unusual, and is related to the estimation error of d_S -covariances at the observation locations. In particular, the variance is inversely proportional to the number of observations per location, regardless of L and h .

4 Analysis of sound data from the BNC

We apply here the proposed method to the “class” dataset described in Section 2. As mentioned, the sound tokens come from 110 distinct locations within Great Britain, which are indicated on the geographical map in Figure 2. Also shown is the triangulation used for the smoothing, where the internal nodes contain the locations of the observations. It can be seen that the observed locations are irregularly spaced in the region, with high density of the observations around London and other large cities and very sparse observations in Wales and central Southern England, for example. In particular, only three locations are available in Scotland and therefore we will not draw strong conclusions about the dialect variation in that country. Figures A3 and A4 in the Appendix show the counties and regions of Great Britain.

While the method allows for a smooth reconstruction of the sound from the mean MFCC (and a few of these reconstructed sounds for the vowel described above can be found as Supplementary Material), we want also to represent the sound variations (and those of the their d_S -covariance) on a map to be able to explore dialect variations. We need therefore to

reduce the dimensionality of the data object. Among the possible alternatives, we choose to project the mean smooth field onto the principal components obtained from the original data because this allows the comparison of the projections of the smooth field estimated using different choices of bandwidth parameters. Concerning the d_S -covariance smoothed field, its variation will be explored by considering the pairwise distances of the estimated d_S -covariance field, and comparison of these distances with those obtained under the assumption that there is no spatial variation in the d_S -covariance field. We will use a Gaussian kernel for all the results of this Section, and we will now discuss the choice of the smoothing parameters.

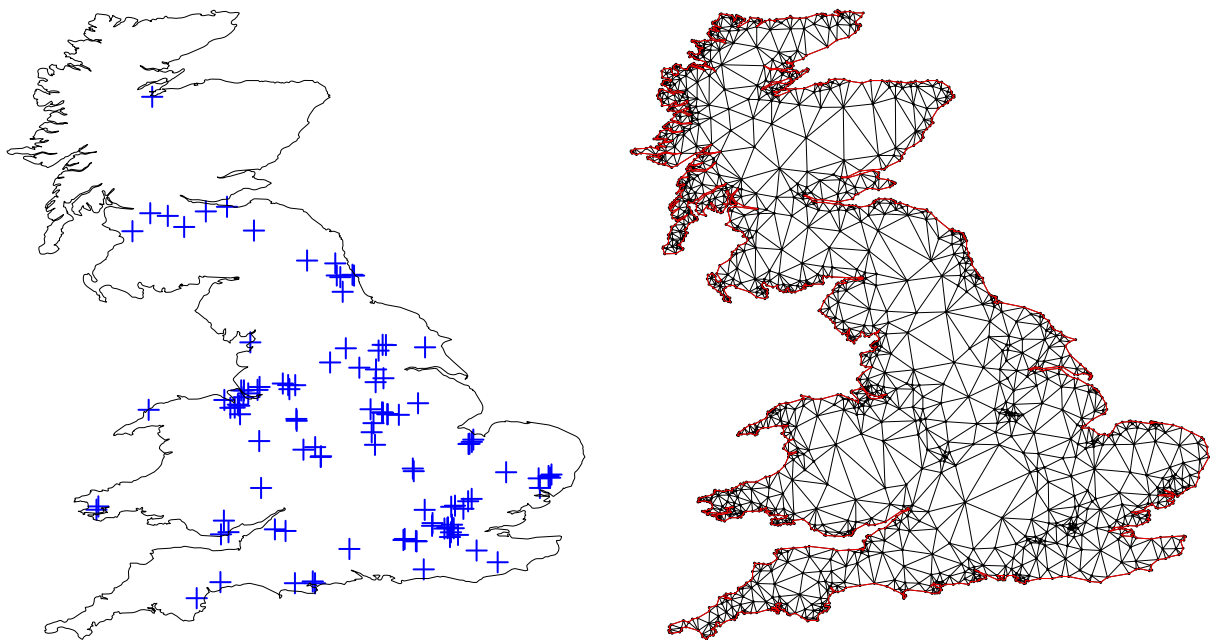


Figure 2: Geographical locations where data are available in the “class” dataset (left) and triangulation of Great Britain (right).

4.1 Choice of Smoothing Parameters

4.1.1 Varying Bandwidths

In both the estimator for the mean and the covariance, a bandwidth varying with the geographical location can be used. This is particularly important when the locations of the observations are irregularly spaced in the region of interest, as is the case for the “class” dataset, where the use of a constant bandwidth would lead to over- or undersmoothed estimates.

A possible approach is to adapt the bandwidth to the density of the observations using

the distance from the k -th nearest *location* to modulate the global bandwidth, i.e.

$$\hbar(x) = h \cdot \Delta_L(x, k), \quad (4.1)$$

where $\Delta_L(x, k)$ is the geographical distance between x and the k -th nearest location to x . This *k -th-nearest locations varying bandwidth* adjusts the bandwidth to the density of the observed locations, thus guaranteeing that information from comparable numbers of observed locations are used in the estimation at each point. However, if there is a large variability between number of observations at different locations, one may prefer to adjust to the number of observations. We can then define a *k -th-nearest observations varying bandwidth* as

$$\hbar(x) = h \cdot \tilde{\Delta}(x, k), \quad (4.2)$$

where $\tilde{\Delta}(x, k)$ is the least distance from x within which there are at least k observations, i.e.

$$\sum_{l: d(x, X_l) < \tilde{\Delta}(x, k)} n_l < k \quad \text{and} \quad \sum_{l: d(x, X_l) \leq \tilde{\Delta}(x, k)} n_l \geq k.$$

A third alternative would be to simply using a fixed bandwidth $\hbar(x) = h$ for all x , but this leads to the problem of oversmoothing in the regions with denser observations, as mentioned above.

The idea of adjusting the bandwidth on the basis of observation density is well known in non-parametric regression (see e.g. Fan & Gijbels 1995), but the difficulty in estimating the bivariate density with a relatively small numbers of observations led us to prefer the use of the distance from the k -th nearest neighbour as proxy for the inverse of the density of the observations, this distance being expected to be small in high density regions and large in low density regions.

The expressions of the bandwidth in (4.1) and (4.2) contain two parameters that need to be chosen: the number k of nearest neighbours to be used to adapt the bandwidth and the global smoothing parameter h . These can be chosen by cross-validation, as described in the next Section.

4.1.2 Cross-validation for varying bandwidth parameters

The choice of the parameters k and h for the varying bandwidths (4.1) and (4.2) can be guided by estimating the prediction error as a function of such parameters using a cross-validation procedure. We propose here to use a leave-one-location-out cross validation for the choice of the parameters k and h . For the mean field, the cross-validation is defined by

$$\text{mean.cv}(k, h) = \sum_{l=1}^L \frac{\|\bar{Y}_l - \hat{m}_{-l}(X_l)\|^2}{\hat{\sigma}^2(X_l)},$$

where \hat{m}_{-l} is the estimate of the MFCC field obtained without all the MFCCs observed at location X_l . Analogously, we can define a cross-validation error for the d_S -covariance estimator as

$$\text{cov.cv}(k, h) = \sum_{l=1}^L \int_0^1 d_S^2(\hat{\Omega}_{-l}(X_l)(t), \check{\Omega}_l(t)) dt,$$

where $\hat{\Omega}_{-l}(X_l)$ is the prediction for the d_S -covariance at location X_l obtained from (3.6) without the observations at location X_l , and $\check{\Omega}_l$ is the sample d_S -covariance at X_l . It is however important also to explore the results visually, using the strategies described in Section 4.2, for different values of the smoothing parameters to be sure that the chosen parameters are not leading to oversmoothing or overfitting.

For the “class” dataset, the cross-validation errors different values of h and k can be found in Figure 3 (for the nearest locations bandwidth) and in Figure A1 of the Appendix (for the nearest observations bandwidth).

For the mean field, the nearest locations bandwidth yields the minimal cross-validation errors, with $h = 0.5$, $k = 14$. The nearest observations bandwidth yields a slightly higher minimal cross-validation error ($h = 1.5$, $k = 300$). As will be seen in Figures 4 and Figure A2 of the Appendix, the nearest location bandwidth yields maps that capture more of the variability of the mean MFCC field, whereas the nearest observations bandwidth seems to be oversmoothing. Therefore, we shall use the varying bandwidth with the nearest locations for the interpretation.

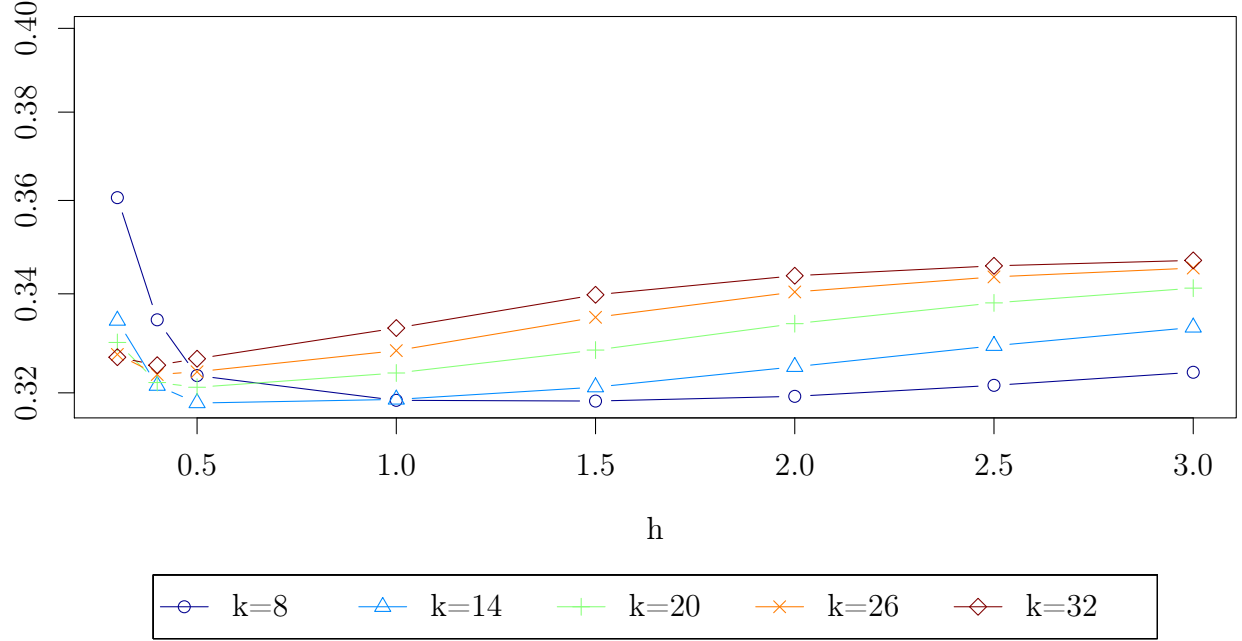
For the d_S -covariance field, the cross-validation curves decrease as the bandwidth parameter h increases, and seem to reach a plateau. We take the smallest value of h (and the corresponding k) that reaches the plateau, which is $h = 1$, $k = 32$ nearest locations. Although the fact that the cross-validation curve reaches a plateau could be an indication that the d_S -covariance field is constant, we shall see in Section 4.3 that there is in fact evidence to support that the d_S -covariance field is not constant.

4.2 Projection of the mean field onto principal components

Visualization of the field of mean MFCC is not a straightforward task. Indeed, at each location x in Great Britain, $\hat{m}(x)$ is an element of $L^2([0, 1], \mathbb{R}^p)$. A visualization of the field \hat{m} can be obtained by projection onto suitable elements of $L^2([0, 1], \mathbb{R}^p)$, i.e. by looking at the map $x \mapsto \langle \hat{m}(x), \varphi \rangle$ for various $\varphi \in L^2([0, 1], \mathbb{R}^p)$. Here we choose to project onto the principal components of the MFCCs $\{Y_{lj} : l = 1, \dots, L; j = 1, \dots, n_l\}$. This allows the reproduction of the geographical variation of the projections which capture most of the variability in the original data and to compare the fields estimated for different values of h and k , the projection directions being independent from them.

The maps of the projections of the estimated field for the choice of h and k that minimises the cross-validation error can be found Figure 4 (this corresponds to the nearest locations bandwidth, with $h = 0.5$, $k = 14$). The maps of projections for the nearest observations bandwidth can be found in Figure A2 of the Appendix. The first principal component direction essentially considers the energy on the second cepstral coefficient, i.e. on the low frequencies. The second principal component essentially considers the energy in the third cepstral coefficient, again energy in the low frequencies. The third principal component direction mainly consists of time dynamics (along the sound length) of the relative volume, and the second and third cepstral coefficients, with some moderate time dynamics in the cepstral coefficients 4 and 5. The fact that most of the energy in the first and second PC loadings concentrate on a single cepstral coefficient confirms that the MFCC representation is

Cross-validation error - nearest locations



Cross-validation error - nearest locations

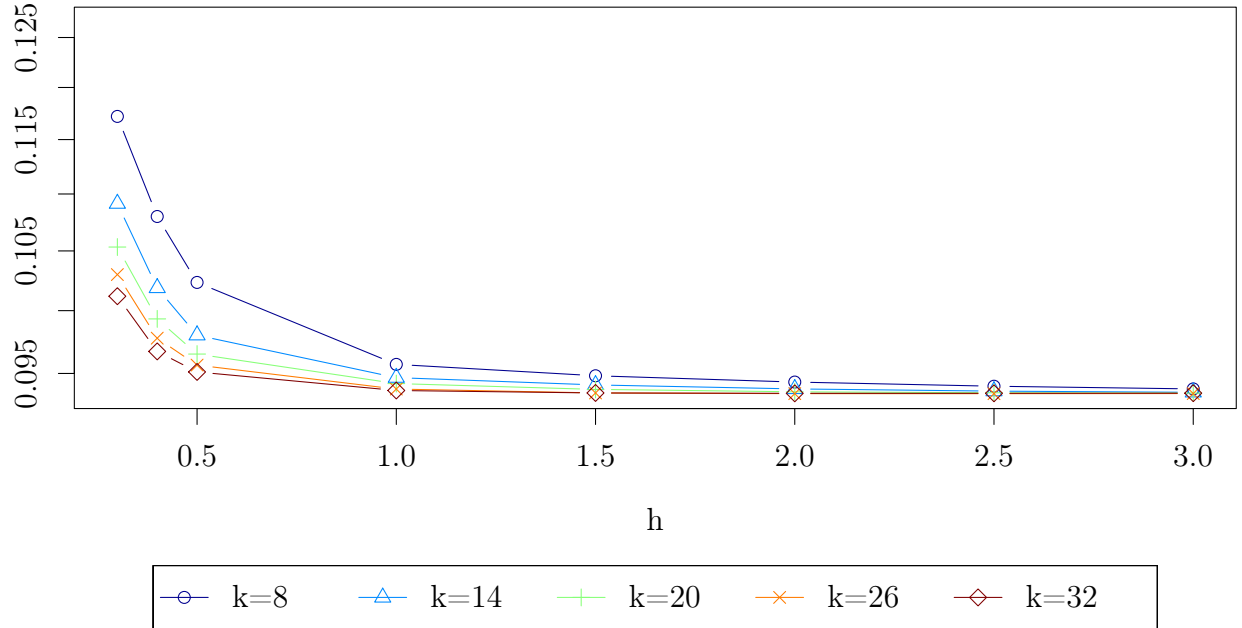
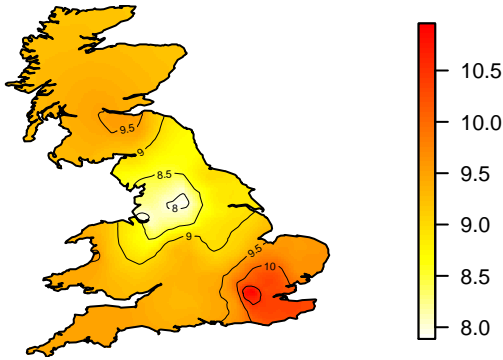
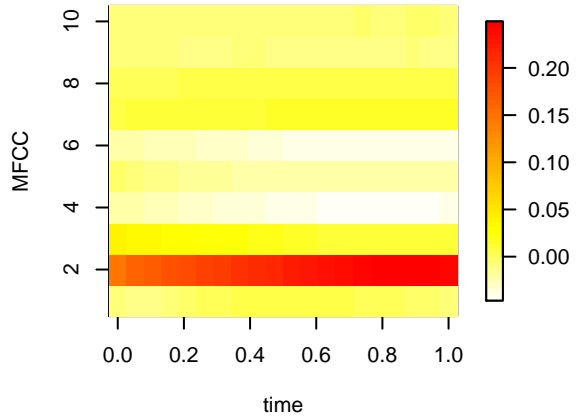


Figure 3: Cross-validation curves of the “class” dataset for the mean MFCC field (top) and the d_S -covariance field (bottom) when the bandwidth is adjusted using the k -th nearest locations.

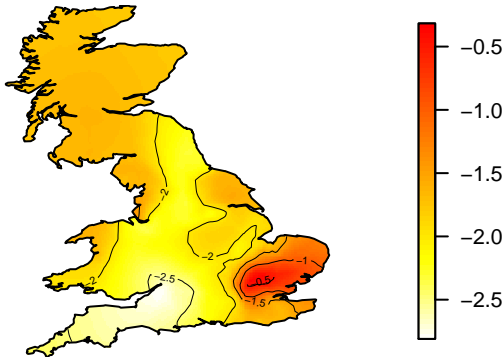
Mean Field projected on PC 1



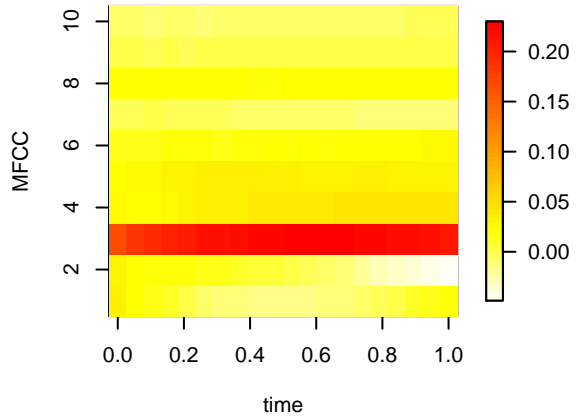
PC 1 loadings



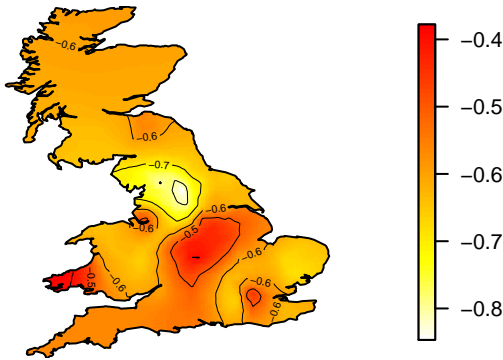
Mean Field projected on PC 2



PC 2 loadings



Mean Field projected on PC 3



PC 3 loadings

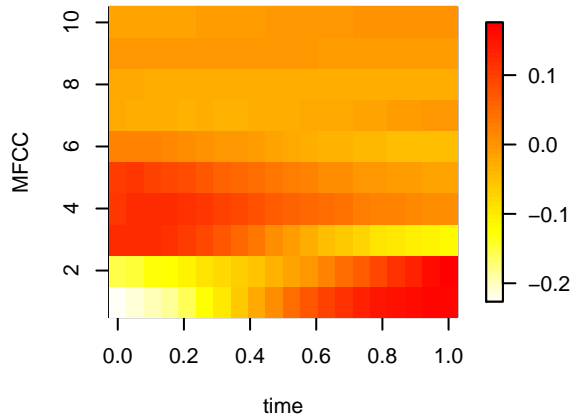


Figure 4: Left: Color maps with contours of the mean smooth MFCC field obtained for the “class” vowel with $h = 0.5$ and $k = 14$ th nearest locations (denoted *NL map* in the text), projected onto the first three principal components directions (from top to bottom) of the original data $\{Y_{lj}(t) : l = 1, \dots, L; j = 1, \dots, n_l\}$. Right: Colour image representing the projection directions (loadings).

indeed a suitable representation for speech sounds. The map of the mean field projected into the first principal component direction highlights the difference between the region around London and the rest of the country, in particular part of North England (and most strongly around Bradford). The projection into the second principal component direction produces high values in East England, and contrasts these values with South West, West Midlands, Yorkshire and the Humber, and North East England, with the strongest contrast being with South West England. The projection in the third principal component direction produces low values in North England, and contrasts this region with isolated regions, such as East Midlands, the London area, and South West Wales. Figures A3 and A4 in the Appendix show the counties and regions of Great Britain, and are provided as geographical aids ¹.

In order to assess whether there is spatial information in the mean field estimate, we compare our estimates with a simulation where the mean and the error terms have no spatial information. The results of the simulation provide evidence in support of spatial structure for the mean field, which is expected since the cross-validation curves have a clear minimum. Details of the simulation are given in Section E of the Appendix.

4.3 MFCC d_S -Covariance Field

While the mean MFCC field captures the information about the average dialect sound changes, the regional variability of such dialect sounds may well also be of considerable interest. We therefore also want to explore how the d_S -covariance changes over the region of interest. While it is in principle possible to use dimension reduction methods, the interpretation of projections of the d_S -covariance may be problematic, as discussed in Section 3.1. An alternative way to represent the d_S -covariance variation is to consider a single location of interest and plot the square-root distances (averaged over the length of the sound) between the d_S -covariance at the location of interest, and the d_S -covariances at all other locations of the map. This produces 2D surfaces that reflect which parts of the country are more similar or dissimilar to the location of interest with respect to d_S -covariance. However, such maps are not directly interpretable, because many of their features appear due to the smoothing method. Indeed, Figure 5 shows the contours of the pairwise distances from Harlow (Essex), overlaid by contours obtained from 100 simulations from a model with constant mean and constant d_S -covariance field (details of the simulations are given in Section E of the Appendix), a procedure which can be considered a bootstrap approximation to the underlying null field. We can see in the Figure that the general form of the contours of the data and the simulations have similar shapes (such systematic effects are not present for the mean MFCC field, as can be seen from Figure A9 of the Appendix). This is because the raw d_S -covariances Ω_l are quite noisy (indeed, Figure A8 in the Appendix, which shows the pairwise distance between the raw d_S -covariances against their corresponding geographical distance, has a nugget). Even though the contours of the data and the simulations have similar shapes, there are some significant differences between them. In Figure 5, we notice that as one moves away from Harlow (Essex), the distances between the d_S -covariances are growing faster in the data than what would be expected if there was no spatial structure in the d_S -covariance

¹The maps shown in this paper do not include the Isle of Wight, located off the south coast of Great Britain, as there is no data present here, and as it is not simply connected to the rest of mainland UK, it is not possible to provide smooth estimates here

field. However, this is not true for all regions of Great Britain. Indeed, Figure 6, which shows the pairwise distances from Morecambe (Lancashire), does not exhibit such features as clearly. In principle, one could look at such maps of contours of distances from each region of Great Britain to assess whether or not the d_S -covariance field is varying spatially, but this is cumbersome and not visually appealing. A more appropriate tool for this purpose is to represent a normalized version $z_D(x, y)$ of the pairwise distances between d_S -covariances at locations x and y . The definition of $z_D(x, y)$ is as follows:

$$z_D(x, y) = \frac{D(x, y) - \overline{D^*}(x, y)}{\sigma^*(x, y)}, \quad (4.3)$$

where $D(x, y)$ is the distance between the d_S -covariances at x and y estimated from the data, $\overline{D^*}(x, y)$, respectively $\sigma^*(x, y)$, is the average, respectively the standard deviation, of $\{D^{*b}(x, y) : b = 1, \dots, 100\}$, where $D^{*b}(x, y)$ is the distance between the d_S -covariances at x and y for the b -th simulation replicate (for both the data and all the simulations, the smoothing parameters are $h = 1$, $k = 32$ nearest locations). The notation $z_D(x, y)$ is chosen because (4.3) can be interpreted as a z-score for the distance between the d_S -covariances between locations x and y of the data, under the null hypothesis that the d_S -covariance field is constant. Figure 7 shows some examples of the surface $\{z_D(x_0, y) : y \in \mathcal{E}\}$, for some $x_0 \in \mathcal{E}$. It is then possible to consider many such surfaces for locations all over Great Britain to get a global appreciation of the variation of the d_S -covariance field. Figure 8 shows the maps associated to many representative locations together with their geographical position in Great Britain, a “map of maps”. We can see in the Figure that there is a very strong indication that the d_S -covariances of the region around Glasgow and Edinburgh are different from those of North England, and that the d_S -covariance of the Midlands are different from those in South and South-West England. There is also very strong indication that the d_S -covariance around Cambridgeshire is different from those of East England and South-East England, and moderate to strong indication that the d_S -covariances of South England are different from those of the rest of England and Wales. All of these interpretations should be of course tempered by the fact that they are drawn from a very crude univariate representation of the d_S -covariance field (namely, the z -scores of their pairwise distances), and while it allows to find regions where the d_S -covariance field is varying spatially, it is not clear if a small value of the z-score $z_D(x, y)$ implies that there is no difference between the d_S -covariances at x and y . Figures A3 and A4 in the Appendix show the counties and regions of Great Britain, and are provided as geographical aids.

5 Discussion

We presented a method to explore spatial variation of sound processes which is of interest in particular for dialectology and comparative linguistics. The need to model the change in the covariability between frequencies, as well as in the mean sound, led us to propose the novel

essex: harlow, uk

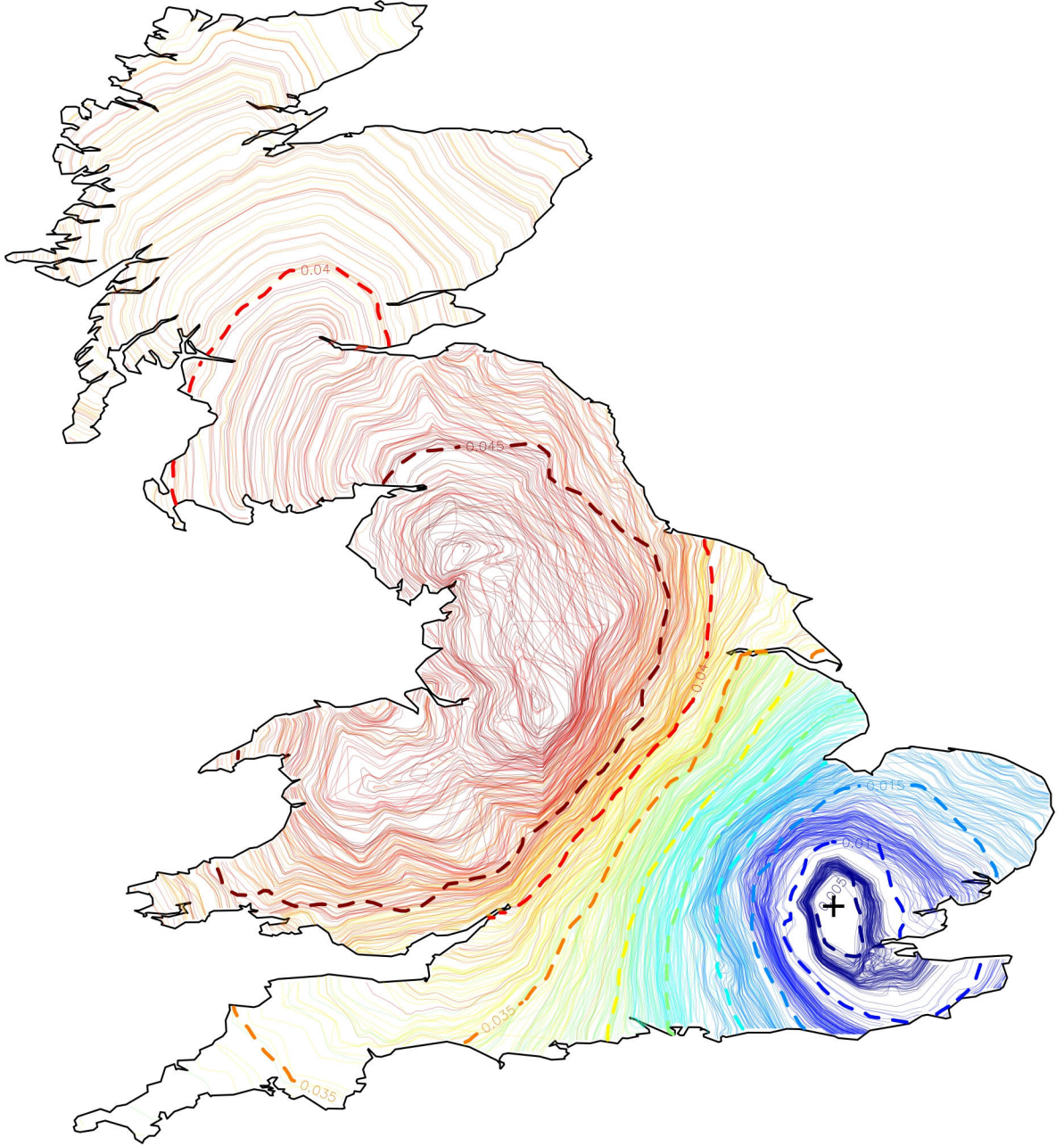


Figure 5: Contours of the pairwise distances between the d_S -covariances at Harlow (Essex), and other location in Great Britain. The thick dashed lines correspond to the contours (level sets) for the BNC data, and the corresponding contours for each of the 100 simulations are given in thin lines, with the corresponding color.

lancashire: morecambe, uk

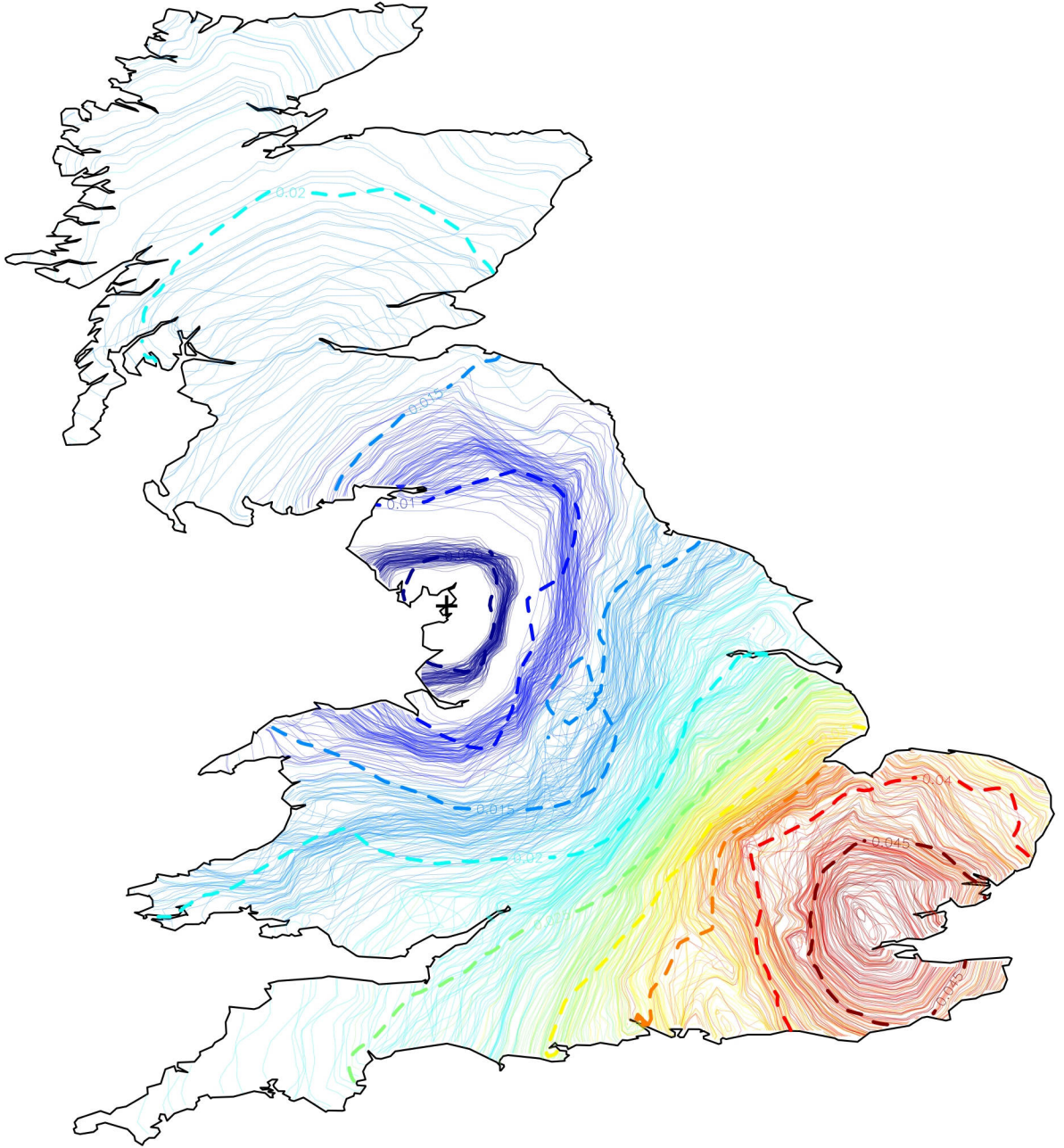


Figure 6: Contours of the pairwise distances between the d_S -covariances at Morecambe (Lancashire), and other location in Great Britain. The thick dashed lines correspond to the contours for the BNC data, and the corresponding contours for each of the 100 simulations are given in thin lines, with the corresponding color.

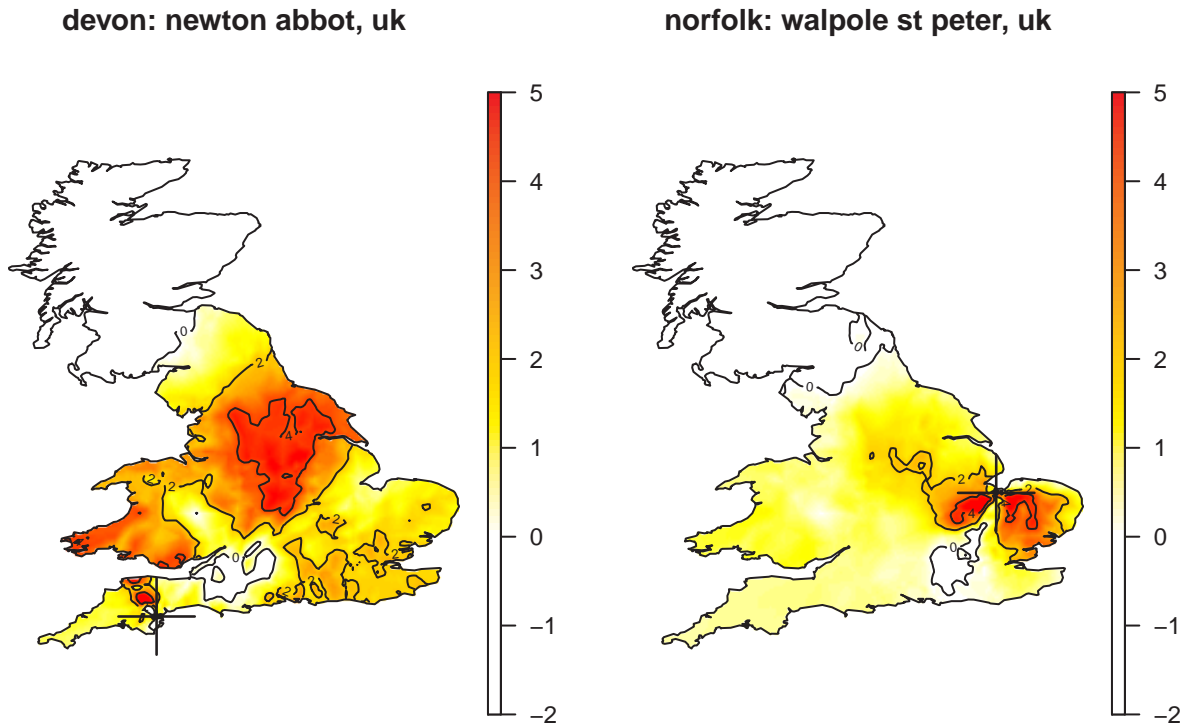


Figure 7: Z-scores $\{z_D(x_0, y) : y \in \mathcal{E}\}$ of the pairwise distances between the d_S -covariances from Poole (Dorset) (left), and from Driffield (right). The “+” on the maps represent the location of the corresponding x_0 . The definition of $z_D(x_0, y)$ is given in (4.3).

statistical concept of d -covariance, i.e. a definition of covariability that relies on a metric distance d different from the Euclidean (Frobenius) distance. This allows the use of metrics that do not produce swelling effects, while estimating the d -covariance consistently in the locations where observations are available. In particular, we chose the square root distance d_S described in Dryden et al. (2009) because it is defined for positive semi-definite matrices, and an explicit expression is available, as we showed in Section 3. It is clear that other metrics could be used within this framework, and indeed recent work on choosing metrics (Petersen & Müller 2016a) and smoothing under general metrics (Petersen & Müller 2016b) could prove relevant to this setting. However it is important to remember that the choice of metric should be considered within a data application context as well.

We used a Mel Frequency Cepstral Coefficients (MFCC) representation for the sound data objects because this has been found empirically to provide a better sound reconstruction, especially in the modified version of the algorithm proposed by Erro et al. (2014). Moreover, the fact that the frequency domain is partitioned into a relatively small number of channels makes this representation more robust to small frequency misalignments across speakers. MFCCs can be then treated as multivariate functional data, and we proposed a model where both the mean and the d_S -covariance between coefficients change smoothly in space. We proposed to estimate these smooth fields with a non-parametric estimator, and showed that this provides consistent estimates both for the mean and for the d_S -covariance field. We also

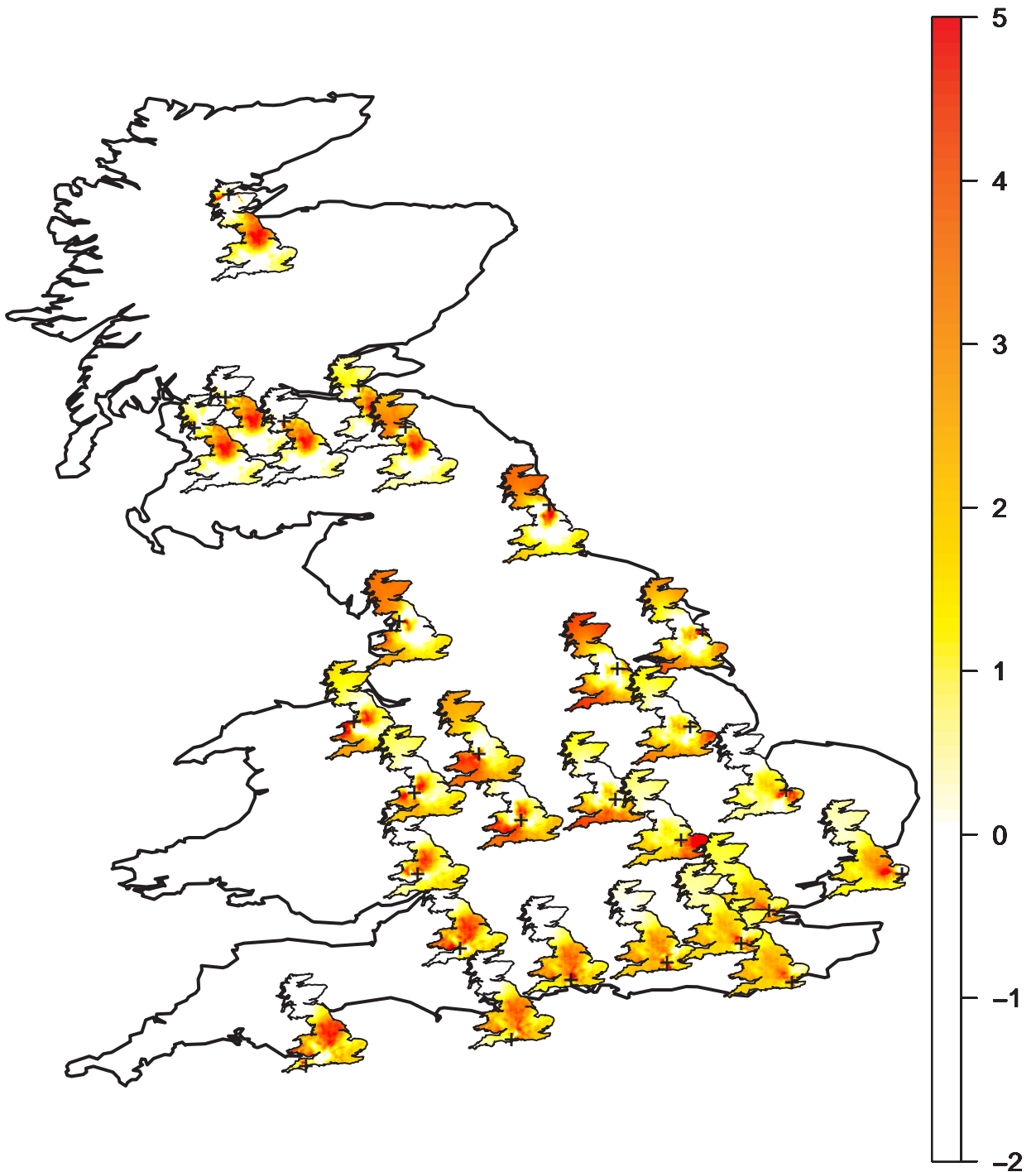


Figure 8: Z-scores $\{z_D(x_0, y) : y \in \mathcal{E}\}$ of the pairwise distances between the d_S -covariances for a number of representative locations x_0 in Great Britain, reported on the corresponding positions on the geographical map of Great Britain. The '+' on the small maps represent the location of the corresponding x_0 . The definition of $z_D(x_0, y)$ is given in (4.3).

integrated into the smoothing procedure a geographical distance based on the shortest path on the mesh used to triangulate the possibly non-convex region of interest. This required a non-trivial argument to show the consistency of the derived estimator and it has a wider applicability wherever there is the need of accounting for a complex geographical domain.

The proposed method allows, for the first time, the sound variation to be studied using speech recordings directly (as opposed to phonetic transcription), and provides a continuous model for the sound change (through its mean and d_S -covariance) in place of discrete regions boundaries, such as those traditionally reported in isoglosses. We analysed speech data from the spoken part of the British National Corpus, and focused on the pronunciation of the vowel in words such as *fast* or *class*, which is known to vary on a dialect basis (Upton & Widdowson 2013), and has particularly prominent variations in British English. While it is possible to listen to the reconstructed sounds (as given in the Supplementary Materials), visual maps are often useful to recognise both global patterns and local features. Exploring the estimated mean and d_S -covariance fields, we uncovered geographical patterns that resemble established findings about the vowel pronunciation (such as the contrast between the North and South-East England). However, the variation appears to be somewhat smoother than expected (i.e. from traditional dialectological maps of 'isoglosses'), to the point where it is possible to identify intermediate regions not easily classified by a hard clustering. This invites additional studies to explore other sounds and further exploration of this and alternative corpora. Indeed, possible immediate extensions for this work include studying the joint behaviour of multiple words/sounds in the language and taking into account additional (non geographical) covariates, such as socio-economic variables.

SUPPLEMENTARY MATERIAL

Supplementary materials (functions used for the smoothing, sample sounds) can be obtained through the authors.

Appendix A Square Root of Symmetric Semi-positive Matrices

We give here some useful properties of square root of matrices. The following result states that square root of a symmetric positive semi-definite matrix is unique.

Theorem A.1 (e.g. Axler (2015)). *Let A be a $p \times p$ real matrix. If A is symmetric positive semi-definite, i.e. $A = A^\top$ and $x^\top A x \geq 0, \forall x \in \mathbb{R}^p$, then there exists a unique positive $p \times p$ matrix B such that $A = BB$. The matrix B is called the square root of A , and is denoted by \sqrt{A} or $A^{1/2}$.*

In particular, this tells us that the square root distance between symmetric positive semi-definite matrices is well defined. The following gives a explicit formula for the square root of symmetric positive semi-definite rank one matrices. It's proof follows from direct calculations.

Proposition A.2. *Let $x \in \mathbb{R}^p, x \neq 0$ and A be a $n \times p$ matrix. Then*

1. $(xx^\top)^{1/2} = xx^\top/|x|$
2. $(Axx^\top A^\top)^{1/2} = Axx^\top A^\top/|Ax|$ provided $Ax \neq 0$.

Appendix B Technical results and proofs

Proof of Proposition 3.2. Without loss of generality, assume that $\mathbb{E}X = 0$. By (3.1), we have $\text{cov}_{d_S}(AX) = \mathbb{E} \left[\frac{AXX^\top A^\top}{|AX|} \right]^2 = A \mathbb{E} \left[\frac{XX^\top}{|AX|} \right] A^\top A \mathbb{E} \left[\frac{XX^\top}{|AX|} \right] A^\top$. The proof is completed by showing that $\text{cov}_{d_{S,A}}(X)$ must satisfy $\text{cov}_{d_{S,A}}(X) = A \mathbb{E} \left[\frac{XX^\top}{|AX|} \right] A^\top A \mathbb{E} \left[\frac{XX^\top}{|AX|} \right] A^\top$, which follows from a straightforward calculation. \square

Proof of Proposition 3.3. Let $\tilde{S} = \left(\frac{1}{n} \sum_{i=1}^n \sqrt{(Y_i - \mu)(Y_i - \mu)^\top} \right)^2$, and $S = \text{cov}_{d_S}(Y)$. Recall that $S = \left(\mathbb{E} \sqrt{(Y - \mu)(Y - \mu)^\top} \right)^2$. Let $\phi_x(y) = \sqrt{(x - y)(x - y)^\top}$, for $x, y \in \mathbb{R}^p$. Notice that $\phi_x(y) = (x - y)(x - y)^\top/|x - y|$ if $y \neq x$, and $\phi_x(x) = 0$. Furthermore, it is not difficult to show that ϕ_x is Lipschitz, i.e. $\|\phi_x(y) - \phi_x(y')\| \leq \kappa_p |y - y'|$, where $\kappa_p \geq 0$ does not depend on the value of x , but only on the dimension p . We therefore have

$$\begin{aligned} d_S(\hat{S}, \tilde{S}) &\leq \frac{1}{n} \sum_{i=1}^n \|\phi_{Y_i}(\bar{Y}) - \phi_{Y_i}(\mu)\| \\ &\leq \frac{1}{n} \sum_{i=1}^n \kappa_p |\bar{Y} - \mu| \\ &= \kappa_p |\bar{Y} - \mu|, \end{aligned}$$

and $d_S(\hat{S}, \tilde{S}) = O_{\mathbb{P}}(n^{-1/2})$.

The proof is completed by showing that $d_S(\tilde{S}, S) = O_{\mathbb{P}}(n^{-1/2})$, which follows from the central limit theorem applied to the random element $\sqrt{(Y - \mu)(Y - \mu)^\top}$. The central limit theorem is indeed applicable here since

$$\begin{aligned} \mathbb{E} \left[\left\| \sqrt{(Y - \mu)(Y - \mu)^\top} \right\|^2 \right] &= \mathbb{E} \left[\left\| \frac{(Y - \mu)(Y - \mu)^\top}{|Y - \mu|} \right\|^2 \right] \\ &= \mathbb{E} |Y - \mu|^2 < \infty. \square \end{aligned}$$

Proof of Theorem 3.7. By the triangle inequality,

$$d_S(\hat{\Omega}(x, t), \Omega(x, t)) \leq d_S(\hat{\Omega}(x, t), \tilde{\Omega}(x, t)) + d_S(\tilde{\Omega}(x, t), \Omega(x, t)), \quad (\text{B.1})$$

where $\tilde{\Omega}(x, t)$ is the same as $\hat{\Omega}(x, t)$, but with the sample mean at the observations replaced by the true mean, i.e. $\tilde{\Omega}(x, t) = \left(\sum_{l=1}^L w_l(x) \sqrt{\tilde{\Omega}_l(t)} \right)^2$,

$$\sqrt{\tilde{\Omega}_l(t)} = n_l^{-1} \sum_{j=1}^{n_l} \sqrt{(Y_{lj}(t) - m_l(t))(Y_{lj}(t) - m_l(t))^\top} = n_l^{-1} \sum_{j=1}^{n_l} \sqrt{\varepsilon_{lj}(t) \varepsilon_{lj}(t)^\top}$$

and $m_l(\cdot) = \mathbb{E} Y_{l1}(\cdot)$.

Let us first look at the first term in (B.1). Writing \mathbb{E}_X for the expectation conditional on X_1, \dots, X_L , the triangle inequality and Hölder's inequality yield

$$\mathbb{E}_X d_S(\hat{\Omega}(x, t), \tilde{\Omega}(x, t)) \leq \sum_{l=1}^L w_l(x) \sqrt{\mathbb{E}_X d_S^2(\check{\Omega}_l(t), \tilde{\Omega}_l(t))}.$$

By arguments in the proof of Proposition 3.3, we have

$$\mathbb{E}_X d_S^2(\check{\Omega}_l(t), \tilde{\Omega}_l(t)) \leq \kappa_p^2 n_l^{-1} \mathbb{E} |\varepsilon(x, t)|^2 \Big|_{x=X_l} \leq \kappa_p^2 c^{-1} n^{-1} \sup_{x \in \mathcal{E}, t \in [0,1]} \mathbb{E} |\varepsilon(x, t)|^2,$$

which is non-random, and independent of t . Since $\sum_l w_l(x) = 1$, we get

$$\mathbb{E}_X d_S(\hat{\Omega}(x, t), \tilde{\Omega}(x, t)) \leq \frac{\kappa_p}{\sqrt{cn}} \sup_{x \in \mathcal{E}, t \in [0,1]} \sqrt{\mathbb{E} |\varepsilon(x, t)|^2}$$

Let us now look at the term $\mathbb{E}_X d_S(\tilde{\Omega}(x, t), \Omega(x, t)) \leq \sqrt{\mathbb{E}_X d_S^2(\tilde{\Omega}(x, t), \Omega(x, t))}$. Since

$$\mathbb{E}_X d_S^2(\tilde{\Omega}(x, t), \Omega(x, t)) = \sum_{r,s=1}^p \mathbb{E}_X \left(\left[\sqrt{\tilde{\Omega}(x, t)} \right]_{rs} - \left[\sqrt{\Omega(x, t)} \right]_{rs} \right)^2,$$

it is enough to control the mean square error of each coordinate of $\sqrt{\tilde{\Omega}(x, t)}$. Notice that $\sqrt{\tilde{\Omega}(x, t)} = \sum_{l=1}^L w_l(x) \sqrt{\tilde{\Omega}_l(t)}$. Therefore we can apply Lemma B.1 for each coordinate $1 \leq r \leq s \leq p$ (by symmetry), with $Z_l(t) = \left[\sqrt{\tilde{\Omega}_l(t)} \right]_{rs}$. Since $\mathbb{E}_X \sqrt{\tilde{\Omega}_l(t)} = \sqrt{\Omega(X_l, t)}$ and

$$\begin{aligned} \text{var}_X \left(\left[\sqrt{\tilde{\Omega}_l(t)} \right]_{rs} \right) &= n_l^{-1} \text{var}_X \left(\frac{\varepsilon(X_l, t)_r \varepsilon(X_l, t)_s}{|\varepsilon(X_l, t)|} \right) \\ &\leq n_l^{-1} \mathbb{E}_X |\varepsilon(X_l, t)|^2 \\ &\leq \frac{1}{cn} \sup_{x \in \mathcal{E}, t \in [0,1]} \mathbb{E} |\varepsilon(x, t)|^2 \end{aligned}$$

the Lemma can be applied with $m(x, t) = \sqrt{\Omega(x, t)}$ and $\|\nu\|_\infty \leq (cn)^{-1} \sup_{x \in \mathcal{E}, t \in [0,1]} \mathbb{E} |\varepsilon(x, t)|^2$. For fixed r, s , the conditional squared bias is bounded by $O_{\mathbb{P}}(h^2)$ and the conditional variance term is bounded by $O_{\mathbb{P}}\left(\frac{1}{nLh^2}\right)$, both bounds being uniform in t . The proof is finished by combining these last results. \square

Lemma B.1. Assume $(X_l, Z_l(t)) \in \mathcal{E} \times L^2([0, 1], \mathbb{R}), l = 1, \dots, L$ are i.i.d., with $X_l \stackrel{\text{iid}}{\sim} f$, and assume $Z_l|X_l$ are i.i.d. with mean $\mathbb{E}[Z_l(t)|X_l] = m(X_l, t)$ and $\text{var}(Z_l(t)|X_l) = \nu(X_l, t)$, and that Conditions 3.4, 3.5 hold. Furthermore, assume

1. For each $t \in [0, 1]$, $m(\cdot, t) : \mathcal{E} \rightarrow \mathbb{R}$ is C^1 , and

$$\|\nabla_x m\|_\infty := \sup_{x \in \mathcal{E}, t \in [0,1]} \left| \frac{\partial m}{\partial x}(x, t) \right| < \infty,$$

2. f is a continuous density on \mathcal{E} ,

3. $\|\nu\|_\infty := \sup_{x \in \mathcal{E}, t \in [0,1]} \nu(x, t) < \infty$ for each $x \in \mathcal{E}$.

Let $\hat{m}(x, t) = \sum_{l=1}^L w_l(x) Z_l(t)$, where $w_l(x)$ is defined in (3.7). Then for each x in the interior of \mathcal{E} , if $f(x) > 0$, we have

$$|\mathbb{E}_X \hat{m}(x, t) - m(x, t)| \leq \frac{2\pi\mu_2(K)\|f\|_\infty\|\nabla_x m\|_\infty c_2^2}{c_1^2 f(x)} [h + o_{\mathbb{P}}(h)], \quad (\text{B.2})$$

and

$$\text{var}_X(\hat{m}(x, t)) \leq \frac{\|\nu\|_\infty}{Lh^2} \left[\frac{c_2^4}{c_1^4 f^2(x)} + o_{\mathbb{P}}(1) \right] \quad (\text{B.3})$$

as $L \rightarrow \infty, h \rightarrow 0$ such that $Lh^2 \rightarrow \infty$, where the remainder terms are uniform in t .

Proof. Without loss of generality, assume that K is renormalized such that $\int_0^\infty K(s) s ds = (2\pi)^{-1}$, and let $\tilde{K}_h : \mathbb{R}^2 \rightarrow [0, \infty)$ be defined by $\tilde{K}_h(x) = K(|x|/h)/h^2 = K_h(|x|)$ for $h > 0$. Notice that \tilde{K}_h is a valid density function on \mathbb{R}^2 for any $h > 0$, and that it is an approximate identity as $h \rightarrow 0$.

We first give a technical result that will be useful, and whose proof follows from standard arguments: for any $\alpha, \beta \geq 0$,

$$\int_{\mathcal{E}} K_h^{1+\alpha}(|x-y|) |x-y|^\beta f(y) dy \leq 2\pi\mu_{\beta+1}(K) \|K\|_\infty^\alpha \|f\|_\infty \cdot h^{\beta-2\alpha}. \quad (\text{B.4})$$

Recall that $\hat{m}(x, t) = \left[\sum_{l=1}^L K_h(d_g(x, X_l)) \right]^{-1} \sum_{l=1}^L K_h(d_g(x, X_l)) Z_l(t)$. First, notice that

$$L^{-1} \left[\sum_{l=1}^L K_h(d_g(x, X_l)) \right] = \int_{\mathcal{E}} K_h(d_g(x, y)) f(y) dy + O_{\mathbb{P}} \left(\left[L^{-1} \int_{\mathcal{E}} K_h^2(d_g(x, y)) f(y) dy \right]^{1/2} \right).$$

By Condition 3.4 and (B.4), the stochastic term is of order $O_{\mathbb{P}}(1/\sqrt{Lh^2})$. Concerning the integral, since K_h is an approximate identity as $h \rightarrow 0$, approximation theory gives

$$\int_{\mathcal{E}} K_h(d_g(x, y)) f(y) dy \geq c_2^{-2} \int_{\mathcal{E}} \tilde{K}_{h/c_2}(x-y) f(y) dy = c_2^{-2} f(x) + o(1)$$

as $h \rightarrow 0$. Therefore, as $h \rightarrow 0, L \rightarrow \infty$,

$$\left[L^{-1} \sum_{l=1}^L K_h(d_g(x, X_l)) \right]^{-1} \leq \frac{c_2^2}{f(x)} + o_{\mathbb{P}}(1). \quad (\text{B.5})$$

Let us now look at the bias term. First, notice that $\mathbb{E}_X \hat{m}(x, t) = \sum_{l=1}^L w_l(x) m(X_l, t)$. Since $x \mapsto m(\cdot, t)$ is C^1 , for all $x, y \in \mathcal{E}$, Taylor's theorem yields $m(y, t) = m(x, t) + r(x, y, t)$, where $|r(x, y, t)| \leq \|\nabla_x m\|_\infty |x - y|$. Therefore, using (B.5),

$$|\mathbb{E}_X \hat{m}(x, t) - m(x, t)| \leq \left[\frac{c_2^2}{f(x)} + o_{\mathbb{P}}(1) \right] \|\nabla_x m\|_\infty \cdot \left[L^{-1} \sum_{l=1}^L K_h(d_g(x, X_l)) |x - X_l| \right]$$

The second term in square brackets is now approximated:

$$\begin{aligned}
L^{-1} \sum_{l=1}^L K_h(d_g(x, X_l)) |x - X_l| &\leq c_1^{-2} L^{-1} \sum_{l=1}^L K_{h/c_1}(|x - X_l|) |x - X_l| \\
&= c_1^{-2} \int_{\mathcal{E}} \tilde{K}_{h/c_1}(x - y) |x - y| f(y) dy \\
&\quad + c_1^{-2} O_{\mathbb{P}} \left(\left[L^{-1} \int_{\mathcal{E}} K_{h/c_1}^2(|x - y|) |x - y|^2 f(y) dy \right]^{1/2} \right) \\
&\leq c_1^{-2} 2\pi\mu_2(K) \|f\|_{\infty} \cdot h + O_{\mathbb{P}}(1/\sqrt{L}).
\end{aligned}$$

Combining these results with (B.5) yields the conditional bias term (B.2).

Concerning the variance, we have

$$\begin{aligned}
\text{var}_X(\hat{m}(x, t)) &= \left[L^{-1} \sum_{l=1}^L K_h(d_g(x, X_l)) \right]^{-2} \cdot L^{-1} \left[\frac{1}{L} \sum_{l=1}^L K_h^2(d_g(x, X_l)) \nu(X_l, t) \right] \\
&\leq \left[\frac{c_2^4}{f^2(x)} + o_{\mathbb{P}}(1) \right] \cdot \|\nu\|_{\infty} L^{-1} c_1^{-4} \left[\frac{1}{L} \sum_{l=1}^L K_{h/c_1}^2(|x - X_l|) \right],
\end{aligned}$$

Where we have used (B.5). For the term in the second square brackets, we have

$$\begin{aligned}
\left[\frac{1}{L} \sum_{l=1}^L K_h^2(|x - X_l|) \right] &= \int_{\mathcal{E}} K_h^2(|x - y|) f(y) dy + O_{\mathbb{P}} \left(\left[\frac{1}{L} \int_{\mathcal{E}} K_h^4(|x - y|) f(y) dy \right]^{1/2} \right) \\
&\leq \|K\|_{\infty} \|f\|_{\infty} h^{-2} + O_{\mathbb{P}}(1/\sqrt{Lh^6}),
\end{aligned}$$

where we have used (B.4). Combining these results yields the conditional variance bound (B.3). \square

The following Lemma gives the approximation error in using the sample total variance in place of the true variance in the estimator of the mean field (3.4). Let $\sigma^2(x) = \mathbb{E} \|\varepsilon(x)\|^2$.

Lemma B.2. *Assume*

$$\sup_{x \in \mathcal{E}} \mathbb{E} \|\varepsilon(x)\|^4 < \infty, \quad (\text{B.6})$$

$$c'n \leq n_l \leq C'n, \quad l = 1, \dots, L, \quad \text{for some constants } c', C', \text{ as } n \rightarrow \infty, \quad (\text{B.7})$$

$$\inf_{x \in \mathcal{E}} \sigma^2(x) > 0 \quad \& \quad \sup_{x \in \mathcal{E}} \sigma^2(x) < \infty. \quad (\text{B.8})$$

Let \hat{m} be defined as in (3.4) and let $\check{m}(x) = \sum_{l=1}^L \lambda_l(x) \bar{Y}_l$, where

$$\lambda_l(x) = \tilde{\lambda}_l(x) / \sum_{l=1}^L \tilde{\lambda}_l(x) \quad \& \quad \tilde{\lambda}_l(x) = n_l K_h(d_g(x, X_l)) / \sigma^2(X_l).$$

Then, for fixed L, h ,

$$|\hat{m}(x, t) - \check{m}(x, t)| \leq O_p(n^{-1/2}) \max_{l=1, \dots, L} |\bar{Y}_l(t)|, \quad \text{as } n \rightarrow \infty.$$

Proof. First, notice that $|\hat{m}(x, t) - \check{m}(x, t)| \leq \max_{l=1, \dots, L} |\bar{Y}_l(t)| |\sum_l w_l(x) - \lambda_l(x)|$. For the rest of the proof, will drop the x to simplify notation, and write w_l instead of $w_l(x)$. Notice that

$$\left| \sum_l w_l - \lambda_l \right| \leq \frac{\sum_l |\tilde{\lambda}_l - \tilde{w}_l|}{s_{\tilde{\lambda}}} + \frac{|s_{\tilde{w}} - s_{\tilde{\lambda}}|}{s_{\tilde{\lambda}}},$$

where $s_{\tilde{w}} = \sum_l \tilde{w}_l$ and $s_{\tilde{\lambda}} = \sum_l \tilde{\lambda}_l$. Using (B.7), we get that

$$\left| \sum_l w_l - \lambda_l \right| \leq (C'/c')^2 \frac{\sum_l |\check{\lambda}_l - \check{w}_l|}{s_{\check{\lambda}}} + (C'/c')^2 \frac{|s_{\check{w}} - s_{\check{\lambda}}|}{s_{\check{\lambda}}}, \quad (\text{B.9})$$

where the “ $\check{\cdot}$ ” entries are the same as the “ $\tilde{\cdot}$ ” entries, but without the n_l s, i.e. $\check{w}_l = K_h(d_g(x, X_l))/\hat{\sigma}^2(X_l)$, and $\check{\lambda}_l = K_h(d_g(x, X_l))/\sigma^2(X_l)$. Using (B.6) and the delta method, we have

$$\check{\lambda}_l - \check{w}_l = K_h(d_g(x, X_l)) \cdot O_{\mathbb{P}}(n^{-1/2}).$$

The first summand in (B.9) is now bounded:

$$\begin{aligned} \frac{\sum_l |\check{\lambda}_l - \check{w}_l|}{s_{\check{\lambda}}} &\leq \frac{O_{\mathbb{P}}(n^{-1/2}) \sum_l K_h(d_g(x, X_l))}{\sum_l K_h(d_g(x, X_l))/\sigma^2(X_l)} \\ &= O_{\mathbb{P}}(n^{-1/2}), \end{aligned}$$

where we have used (B.8). Using the same arguments, we get the same bound on the second summand of (B.9),

$$\frac{|s_{\check{w}} - s_{\check{\lambda}}|}{s_{\check{\lambda}}} \leq O_{\mathbb{P}}(n^{-1/2}).$$

The proof is finished by combining these results. \square

Appendix C Data Preprocessing

We describe here in further detail the preprocessing of the sound data extracted from the spoken part of the British National Corpus and analyzed in the paper.

C.1 Raw Data Preprocessing

First all the segmentation information and all the contextual information were extracted. Then, the list of words for the segmentation and the context were corrected for coding differences (e.g. “they’ll” was coded as two separate words “they” and “ll” in the contextual information files). After this, the segmentation and contextual information were merged together. This was done by matching—within each audio recording file—consecutive groups of words. The algorithm we used looked for a unique sequence of words of length L that perfectly matched between the two sets of words. The algorithm looped through the sequence of utterances (sequence of words pronounce by the same speaker) defined in the contextual

XML files, by initially setting L to the minimum of the length of the utterance and 50 (this was chosen for speeding up the matching). If multiple matches were found, L was increased and the search was performed again. If no match was found, L was decreased and the search was performed again. If the algorithm didn't find any match, or if $L > 50$, the algorithm went to the next word in the current utterance (setting $L = 1$). Then L was either increased, respectively decreased, if multiple matches, respectively no match, was found. If $L > 50$, the algorithm was restarted with $L = 1$ but the perfect matching was relaxed to approximate matching using the *optimal string alignment* metric (van der Loo 2014), with distance at most 2.

The result of the preprocessing is a data frame with variables `word`, `begintime`, `endtime`, `textgridfilename`, `index`, `agegroup`, `role`, `sex`, `soc`, `dialecttag`, `age`, `persname`, `occupation`, `dialect`, `id`, `placename`, `activity`, `locale`, `wavfile`, `placenamecleaned` and about 5 million observations (i.e. words). Discriminative information about the speaker is missing for about 2.9% of the words, and information about the location of the recording is missing for about 8.4% of the words.

C.2 Cleaning

Since the data we analyzed are sounds from noisy recording, we first cleaned the sounds corresponding to the set of words

$$\text{class, glass, grass, past, last, brass, blast, ask, cast, fast, pass.} \quad (\text{C.1})$$

The following sounds were removed:

1. Sounds with duration outside the interval $[0.2, 1]$ seconds.
2. 400 sounds with the lowest maximal amplitudes.
3. Sounds corresponding to young speakers (selected by taking speakers less than 10 year old and whose median pitch was above a fixed threshold)

To further remove low quality sounds from our analysis, we ranked the sounds s_1, \dots, s_N , for each word w in (C.1), according to following score,

$$\text{score}_i = \frac{1}{L_i} \sum_{l=1}^{L_i} \left(\check{s}_i(t_l) - \mathbf{1}_{[a(w), b(w)]}(t_l/t_{L_i}) \right)^2 \exp \left(-\mathbf{1}_{[a(w), b(w)]}(t_l/t_{L_i}) \right), \quad (\text{C.2})$$

where $\check{s}_i(t_l) = \tilde{s}_i(t_l) / \max_{l=1, \dots, L_i} \tilde{s}_i(t_l)$, \tilde{s}_i is the root mean square amplitude (RMSA) of s_i on a running window of 10 milliseconds, and $a(w), b(w) \in [0, 1]$ were chosen by looking at the plot of \tilde{s}_i for a sound of good quality, and correspond roughly to the location of the vowel in the sound. Large values of score_i correspond to noisier sounds. The effect of the exponential factor in (C.2) is to give higher score to sounds having large RMSA outside the vowel interval, while still penalizing for low RMSA inside the vowel interval. For each word w of our list of words, we then discarded the sounds with the largest 5% scores.

C.3 Vowel Segmentation and MFCC Extraction

We extracted the MFCCs of all the sounds corresponding to the words in (C.1), using the software `ahocoder` (<http://aholab.ehu.es/ahocoder/index.html>) with parameter `--CCORD=30 --LFRAME=16`.

In order to extract the MFCC corresponding to the vowel segment of the recording of the words in (C.1), we performed the following steps. For each word in (C.1):

1. align the MFCCs of the sounds of the word with respect to the first MFCC coefficient,
2. find the segment of the warped sounds which corresponds to the vowel,
3. extract the corresponding portion on the unwarped MFCCs,
4. recompute all the unwarped MFCCs on a common grid,

C.4 MFCC alignment

Let us describe more precisely the alignment step in the preprocessing procedure. Let $\text{MFCC}_i(t, m), i = 1, \dots, N$ denote the MFCCs of the sounds corresponding to the current word w . Recall that $m = 1, \dots, M$, and assume that the time domains have been linearly rescaled, i.e. $t \in [0, 1]$. We first align the curves $\text{MFCC}_i(\cdot, 1), i = 1, \dots, N$ using the Fisher-Rao metric. This yields warping functions $\gamma_i : [0, 1] \rightarrow [0, 1]$ such that $\text{MFCC}_i(\gamma_i(\cdot), 1), i = 1, \dots, N$ are aligned. Then we align all the MFCC coefficients of the sound i using the warping γ_i , that is, we set $\widetilde{\text{MFCC}}_i(t, m) = \text{MFCC}_i(\gamma_i(t), m), t \in [0, 1], m = 1, \dots, M$ for all i . The idea is that, after alignment, the temporal location of the vowel would be the same across all registered MFCCs of a same word, which would make the vowel segmentation much easier.

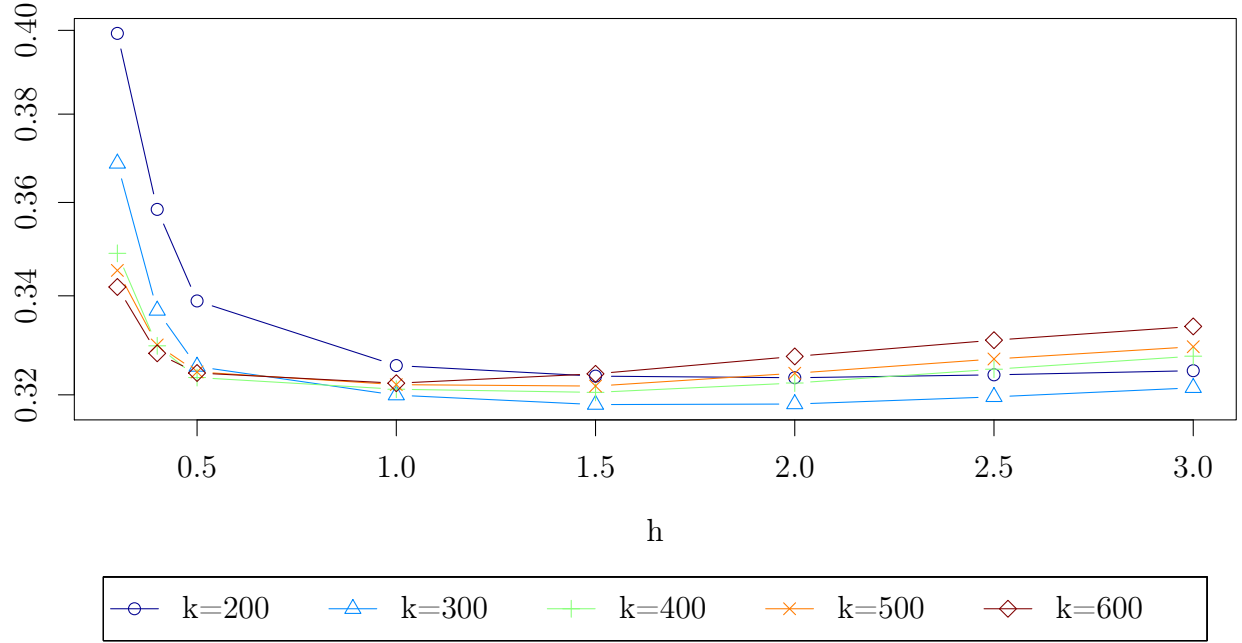
Once the MFCCs corresponding to a common word w have been aligned, the interval $[a(w), b(w)] \subset [0, 1]$ corresponding to the vowel sound was found by manual auditory discrimination. The inverse of the warping functions were then used to compute the interval $I_i = [\gamma_i^{-1}(a(w)), \gamma_i^{-1}(b(w))]$, which is the vowel interval of the i -th unaligned MFCCs. The interval I_i was then linearly rescaled to $[0, 1]$, yielding the vowel MFCCs

$$\text{MFCC}_i^{\text{vowel}}(t, m) = \text{MFCC}_i\left((1-t)\gamma_i^{-1}(a(w)) + t\gamma_i^{-1}(b(w)), m\right), \quad t \in [0, 1] \quad (\text{C.3})$$

Appendix D Modeling the Vowel Sound Duration

The sound duration of the vowel in the words of the “class” dataset are believed to carry part of the information of the spatial variation of the dialect sounds. However, since the duration cannot capture time dynamics in relative volume, and differences in the vowel quality, the information carried by the vowel duration is a very crude approximation of the

Cross-validation error - nearest observations



Cross-validation error - nearest observations

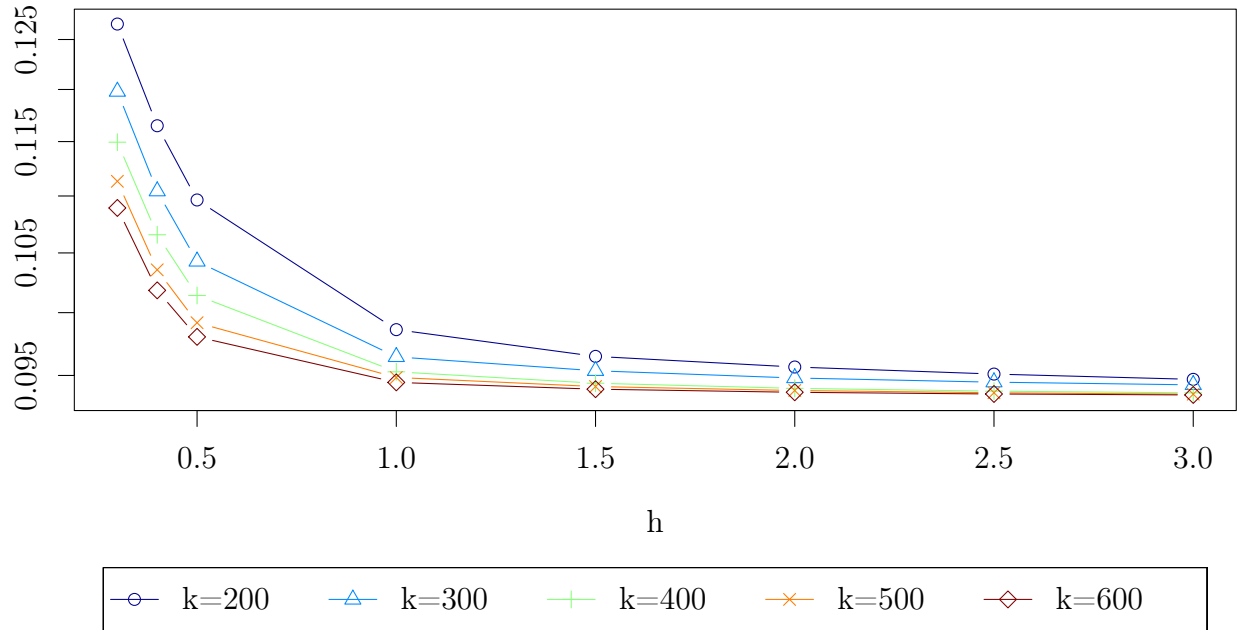
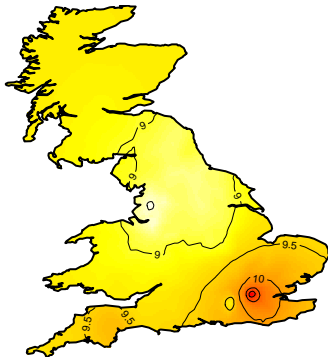
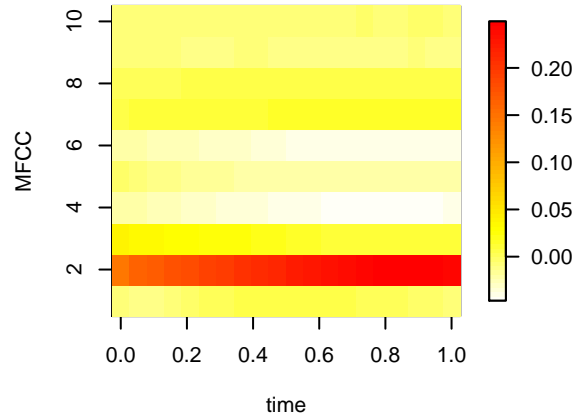


Figure A1: Cross-validation curves of the “class” dataset for the mean MFCC field (top) and the d_S -covariance field (bottom) when the bandwidth is adjusted using the k -th nearest observations.

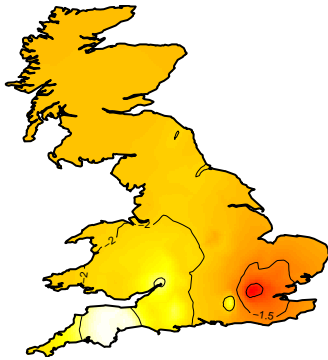
Mean Field projected on PC 1



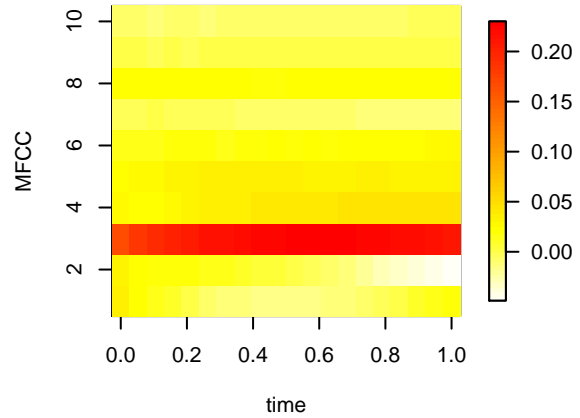
PC 1 loadings



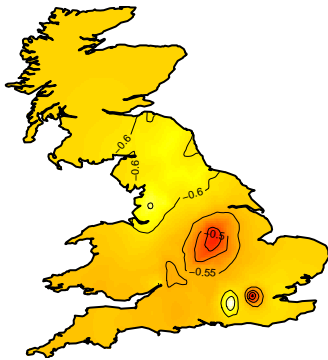
Mean Field projected on PC 2



PC 2 loadings



Mean Field projected on PC 3



PC 3 loadings

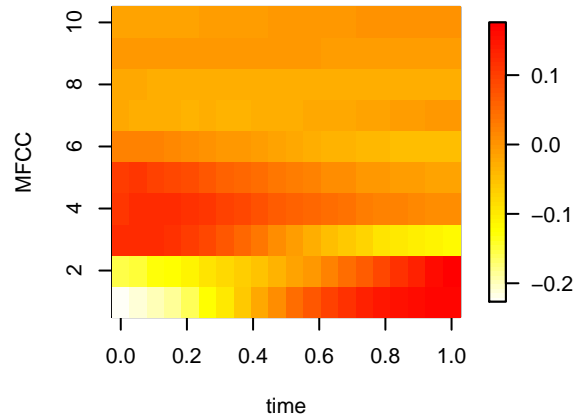


Figure A2: Left: Color maps with contours of the mean smooth MFCC field obtained for the “class” vowel with $h = 1.5$ and $k = 300$ th nearest observations (denoted *NO map* in the text), projected onto the first three principal components directions (from top to bottom) of the original data $\{Y_{lj}(t) : l = 1, \dots, L; j = 1, \dots, n_l\}$. Right: Colour image representing the projection directions (loadings).

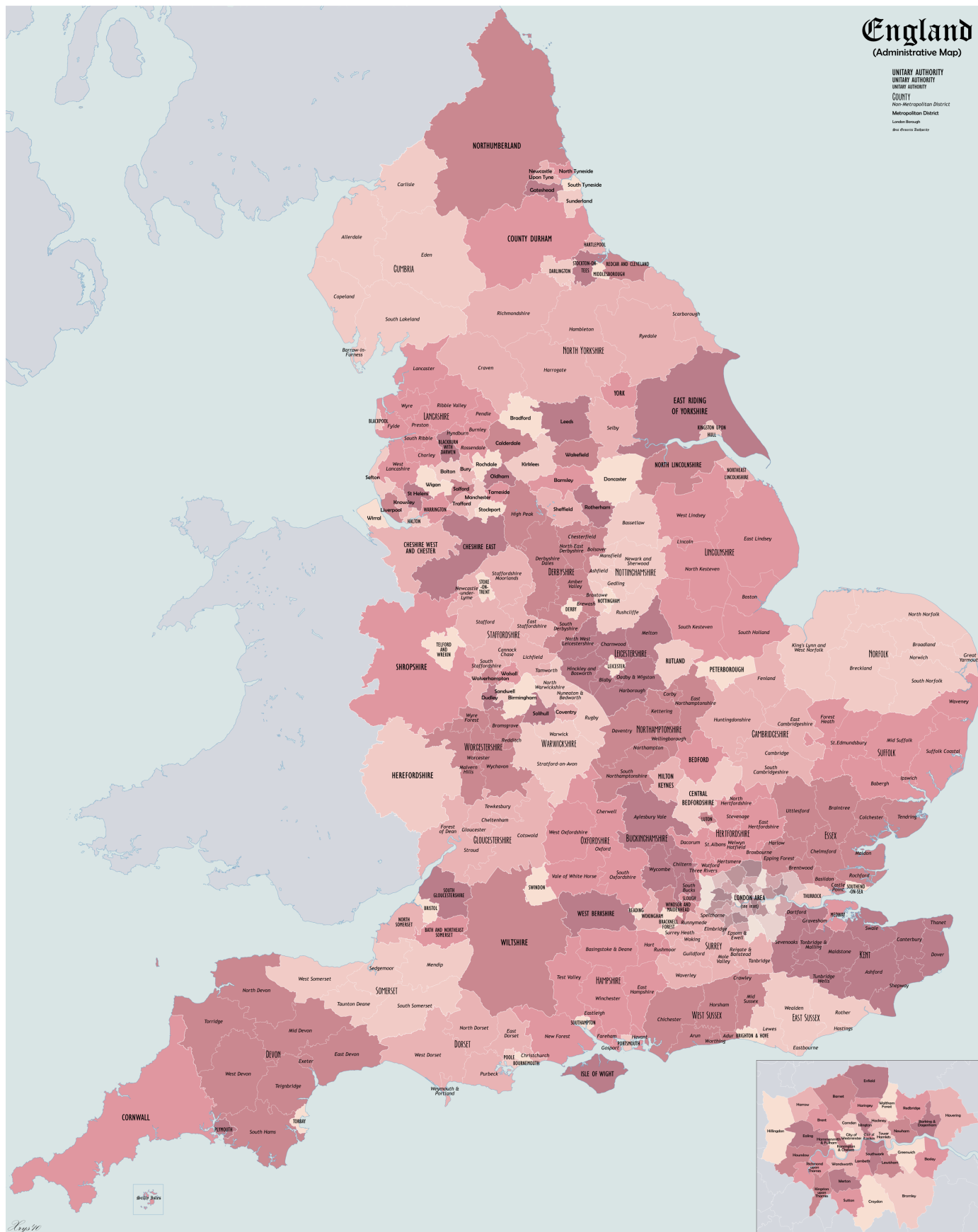


Figure A3: Counties of England. Licenced under the Creative Commons Attribution 3.0 Unported license. Attribution: Xrysd.

https://en.wikipedia.org/wiki/File:England_Administrative_2010.png

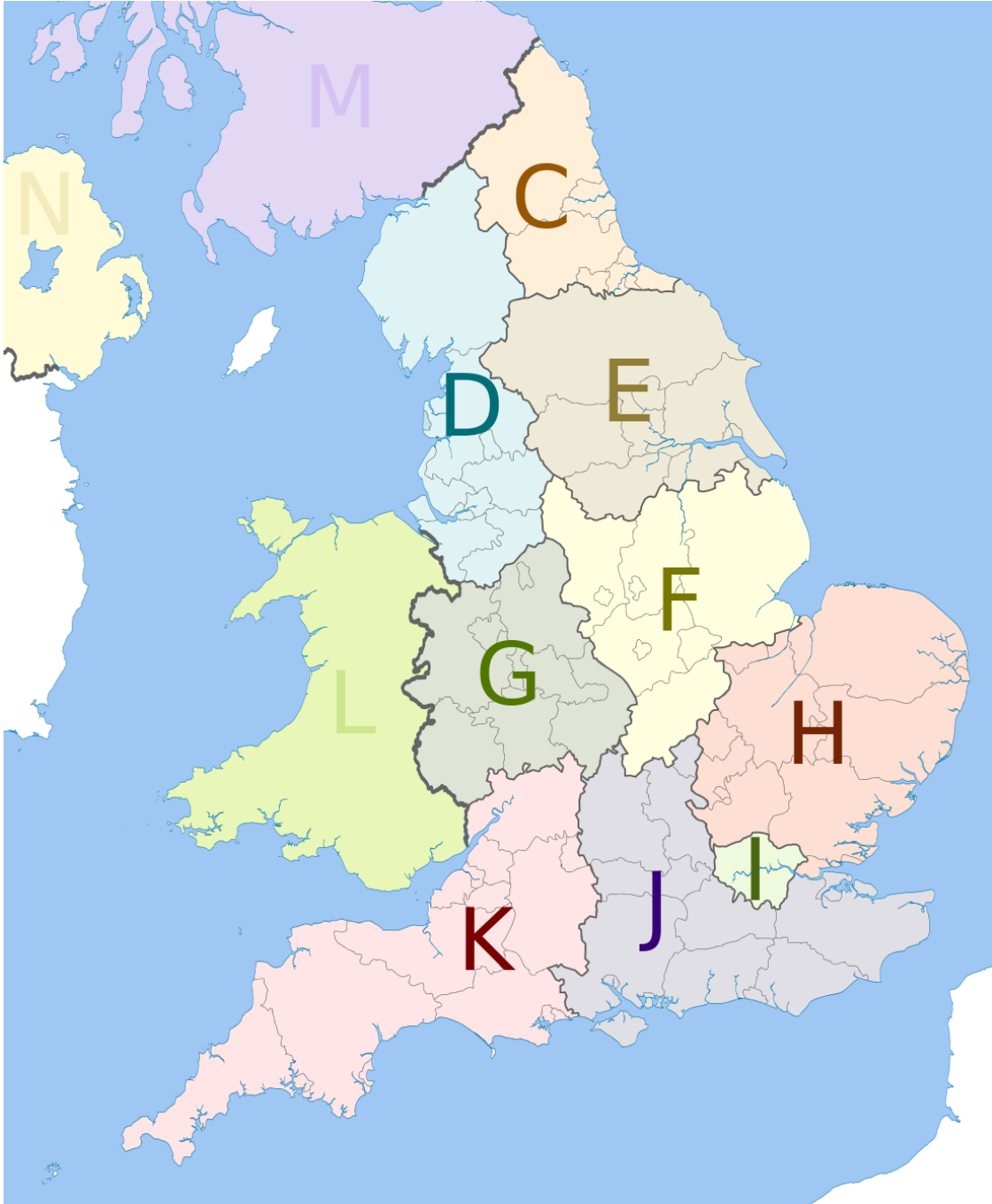


Figure A4: Regions of Great Britain. C = North East England, D = North West England, E = Yorkshire and the Humber, F = East Midlands, G = West Midlands, H = East of England, I = Greater London, J = South East England, K = South West England, L = Wales, M = Scotland. Licenced under the Creative Commons Attribution-Share Alike 3.0 Unported license. Attribution: Dr Greg and Nilfanion.

https://commons.wikimedia.org/wiki/File:NUTS_1_statistical_regions_of_England_map.svg.

vowel sound. This is why the focus of the paper is on the MFCCs of the vowel sounds. We have nevertheless produced a spatial map of the relative duration of the vowel sound (relative to the duration of the word), where the spatial map is obtained by spatial smoothing of the relative durations at each observation location, obtained using a linear mixed model with **observation location**, **word** and **sex** as fixed effects, and **speaker** as random effect. The resulting map is given in Figure A5, together with the projection of the mean MFCC field onto the second principal component. The same spatial smoothing parameters have been used for both maps ($h = 0.5, k = 14$ nearest locations). It can be seen that the two maps are quite correlated (the absolute correlation is 0.66; note that the principal component is defined up to a sign), and therefore the duration information is more or less similar to that obtained by the projection of the MFCC mean field onto the second principal component.

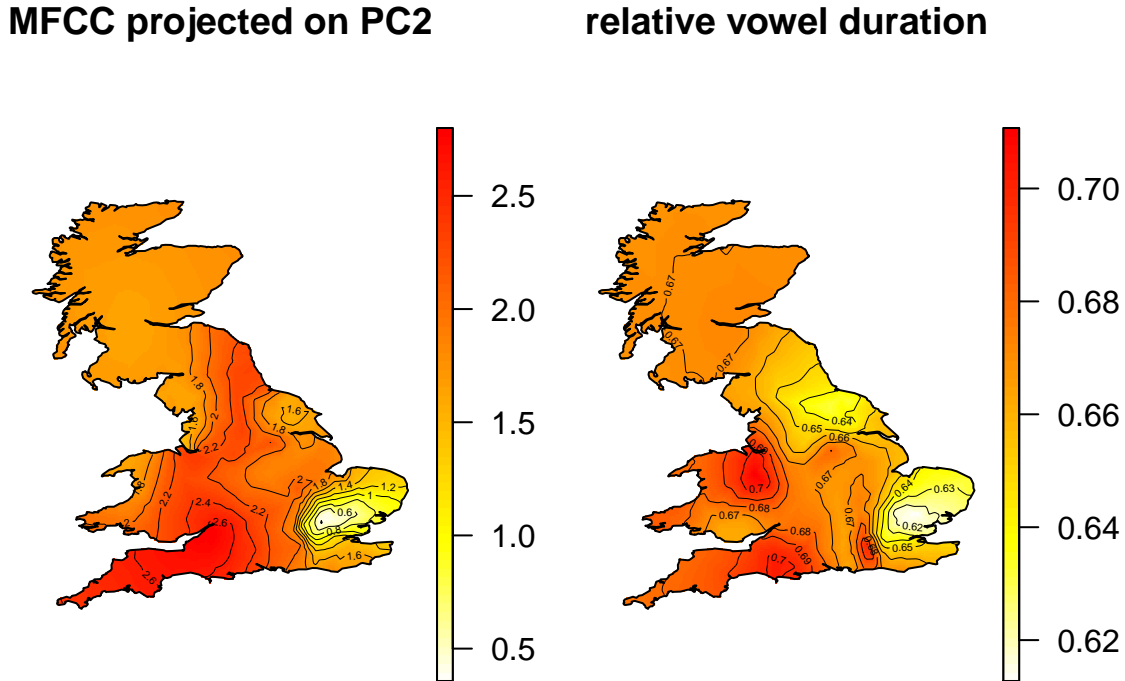


Figure A5: Mean MFCC field projected on PC2 (left) and duration field of the vowel sounds (right). The absolute correlation between the two fields is 0.66.

Appendix E Simulation Study

In order to quantify whether the spatial mean function and the spatial d_S -covariance contain valuable spatial informations, we compare the results obtained in the main paper with a

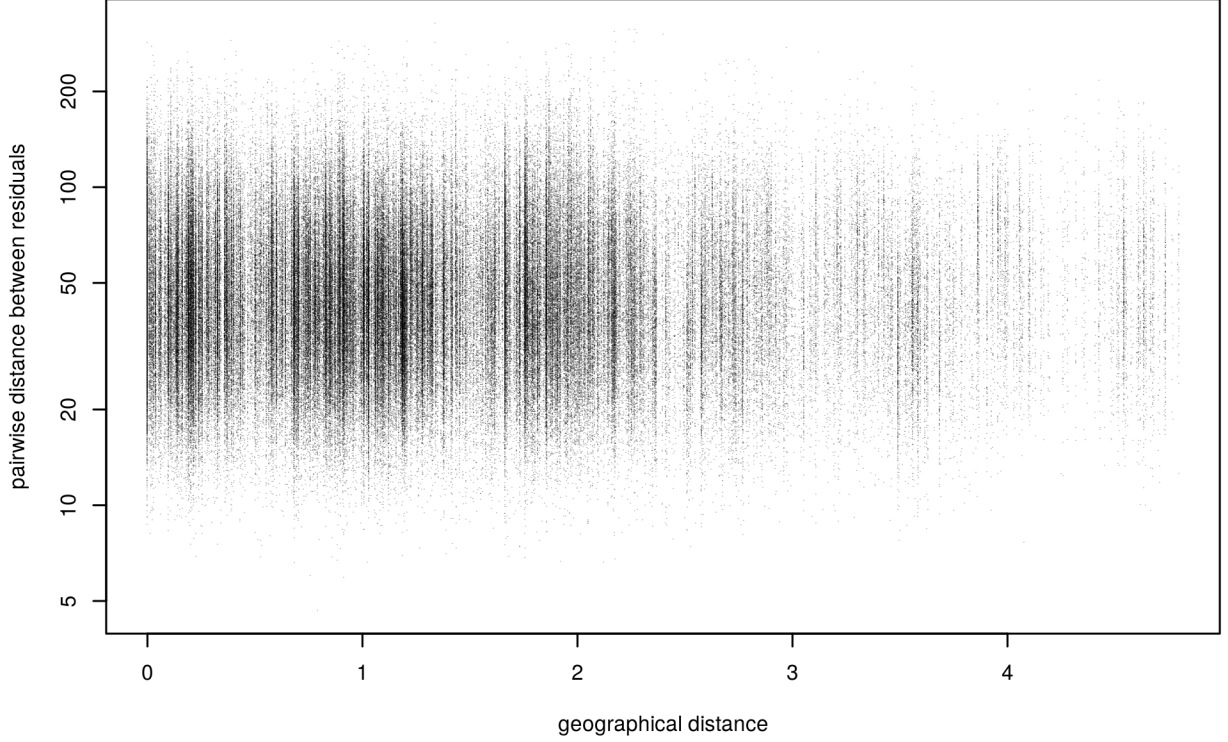


Figure A6: Scatterplot of pairwise distance between residuals (y axis) against their geographical distance (x axis).

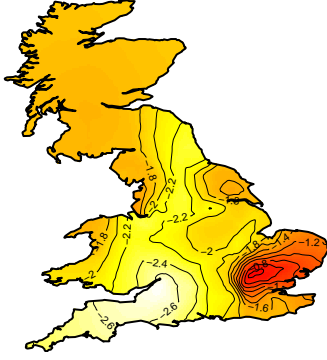
simulation scenario in which all the spatial locations have the same mean and d_S -covariance. We simulate observations from a model with constant mean and constant d_S -covariance,

$$Y_{lj}^* = \mu + \varepsilon_{lj}^*, \quad l = 1, \dots, L; j = 1, \dots, n_l \quad (\text{E.1})$$

where ε_{lj}^* were drawn with replacement from $\{\check{\varepsilon}_{lj} : l = 1, \dots, L; j = 1, \dots, n_l\}$, $\check{\varepsilon}_{lj} = \hat{\varepsilon}_{lj} - \left(\sum_{l,j} \hat{\varepsilon}_{lj}\right) / \sum_l n_l$, $\hat{\varepsilon}_{lj} = Y_{lj} - \hat{m}(X_l)$, where \hat{m} is the estimated of the mean MFCC field obtained from the data with tuning parameters $h = 1, k = 300$ nearest observations, and n_l is the number of observations at location X_l .

The projections onto PC1-3 are given in Figure A9. If there was no spatial information in the mean field of the BNC dataset, the mean field (projected onto PC1) of the simulated data would have the same range of variation as the mean field of the BNC dataset (projected onto PC1). However, the MFCC field of the estimated MFCC field of the simulation has consistently a much smaller range than the smooth field obtained from the BNC dataset over the 100 simulation replicates (the range for the projection on PC1 is $[9.2, 9.7]$ for a realization from (E.1), as opposed to $[7.9, 10.8]$ for the real data application). This provides evidence in support of spatial structure for the mean field.

Mean Field projected on PC 2



Mean Field projected on PC 2

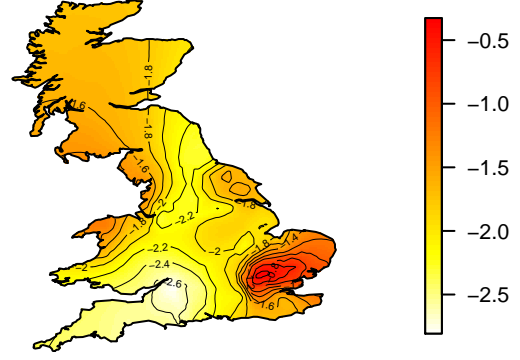


Figure A7: Mean field of the BNC dataset projected on PC2 with computed with geodesic distance (left) and with Euclidean distance (right). Notice the artifacts near the boundaries (the level curves go across the port of Edinburgh when using the Euclidean metric).

Appendix F An illustration of the advantage of the d_S -covariance

As a motivation for the use of d_S -covariances, here is a one-dimensional example which illustrates the advantages of using them when smoothing spatially under the metric d_S . Suppose you have data $Y_{11}, \dots, Y_{1m} \stackrel{\text{iid}}{\sim} \varepsilon(x_1)$ and $Y_{21}, \dots, Y_{2m} \stackrel{\text{iid}}{\sim} \varepsilon(x_2)$, where $x_1, x_2 \in \mathbb{R}$ are two points that are equally close to $x_0 \in \mathbb{R}$, and we wish to estimate the co-variation of $\varepsilon(x_0)$. Assume that $\varepsilon(x) \sim N(0, \sigma^2)$ for all $x \in \mathbb{R}$, and that the mean of $\varepsilon(x)$ is known to be equal to zero. If we wish to estimate the parameter $\sigma^2 = \text{var}(\varepsilon(x_0))$, then a natural estimator is the Fréchet mean of $\hat{\sigma}_i^2 = m^{-1} \sum_{j=1}^m Y_{ij}^2, i = 1, 2$, under d_S , i.e.

$$\hat{\sigma}_*^2 = \left[\left(\sqrt{\hat{\sigma}_1^2} + \sqrt{\hat{\sigma}_2^2} \right) / 2 \right]^2.$$

But

$$\begin{aligned} \mathbb{E} \hat{\sigma}_*^2 &= \mathbb{E}(\hat{\sigma}_1^2 + \hat{\sigma}_2^2)/4 + \mathbb{E} \sqrt{\hat{\sigma}_1^2 \hat{\sigma}_2^2}/2 \\ &< \sigma^2/2 + \sqrt{\mathbb{E} \hat{\sigma}_1^2 \mathbb{E} \hat{\sigma}_2^2}/2 \\ &= \sigma^2/2 + \sqrt{\mathbb{E}(\hat{\sigma}_1^2) \mathbb{E}(\hat{\sigma}_2^2)}/2 \\ &= \sigma^2, \end{aligned}$$

where we have used Jensen's inequality in the second line (which is in this case a strict inequality, since $\hat{\sigma}_1^2 \hat{\sigma}_2^2$ is not almost surely constant), and the independence of $\hat{\sigma}_1^2$ and $\hat{\sigma}_2^2$ in the third line. In other words, $\hat{\sigma}_*^2$ is a biased estimator of σ^2 . Furthermore, since $\sqrt{\hat{\sigma}_1^2}$ and $\sqrt{\hat{\sigma}_2^2}$ are both Chi distributed with m degrees of freedom, $\mathbb{E} \sqrt{\hat{\sigma}_*^2} = \sigma \sqrt{2} \Gamma((m+1)/2) / \Gamma(m/2)$,

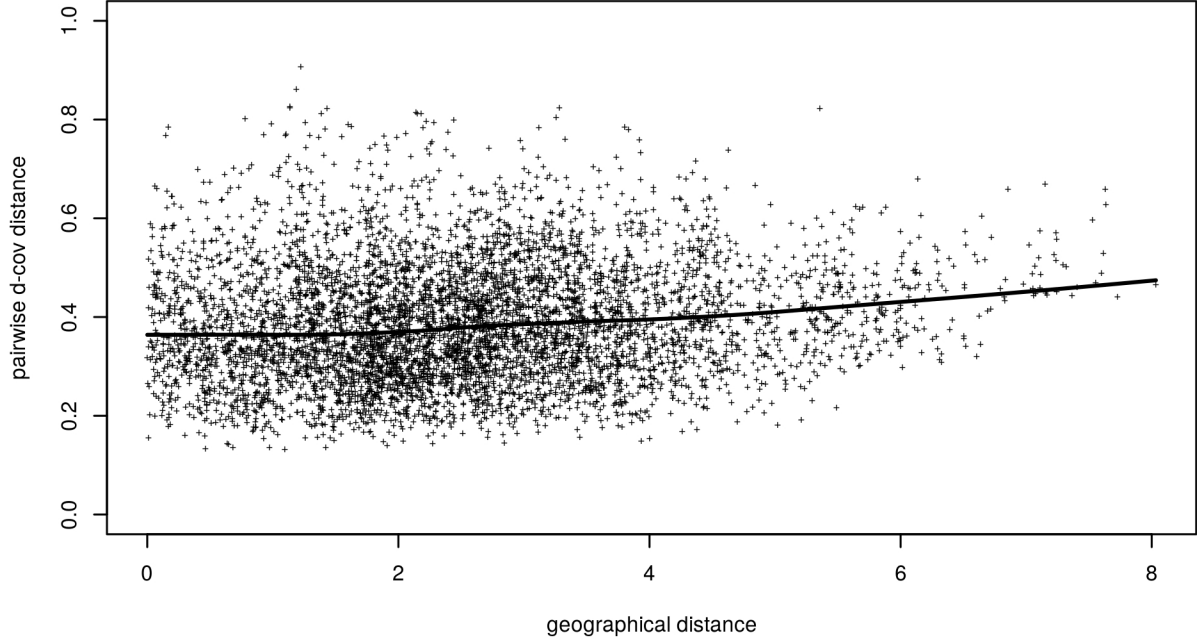


Figure A8: Scatterplot of the distances between the raw d_S -covariances $\check{\Omega}_l, \check{\Omega}_k$, and the corresponding geographical distance between X_l, X_k . Notice that the thick line, which represents a robust local linear regression obtained via the R function `lowess`, has a nugget, and is slightly increasing with the geographical distance.

where Γ is the Gamma function, $\Gamma(z) = \int_0^\infty x^{z-1} e^{-x} dx$, that is, $\sqrt{\hat{\sigma}_*^2}$ is a biased estimator of $\sqrt{\sigma^2}$. In other words, if one smooths the sample variances using the square-root Euclidean metric, the resulting estimator is biased, even in the square-root space. However, if one wishes to estimate the parameter $\tau = \text{cov}_{d_S}(\varepsilon(x_0)) = [\mathbb{E} |\varepsilon(x_0)|]^2$, then the natural estimator is the Fréchet mean of

$$\hat{\tau}_i = \left(m^{-1} \sum_{j=1}^m |Y_{ij}| \right)^2, \quad i = 1, 2$$

under d_S , that is

$$\hat{\tau}_* = \left[(2m)^{-1} \sum_{j=1}^m (|Y_{1j}| + |Y_{2j}|) \right]^2,$$

which is unbiased in the square-root space, i.e. $\mathbb{E} \sqrt{\hat{\tau}_*} = \sqrt{\tau}$. In conclusion, using the same metric for the spatial smoothing and the definition of the co-variation yields estimators that are less biased than those obtained by using distinct metrics.

Mean Field projected on PC 1

Mean Field projected on PC 2

Mean Field projected on PC 3

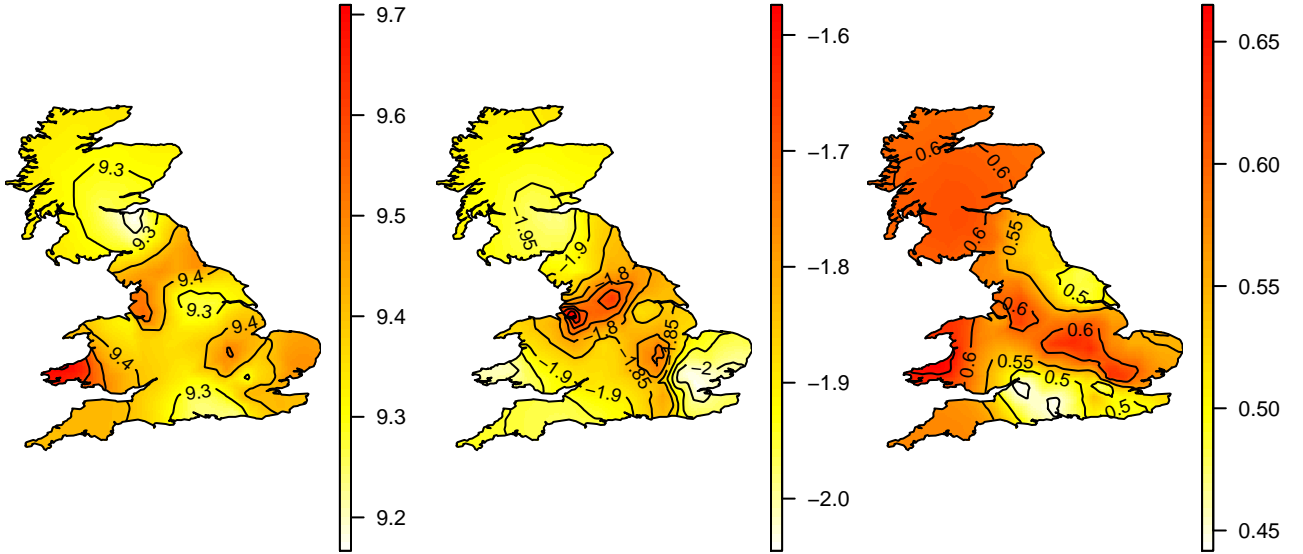


Figure A9: Projection onto PCs 1,2,3 of the mean obtained from data simulated under the global model (E.1)

F.1 Comparison of the d -covariance field under the square-root metric and the Euclidean metric

One might raise the question of whether the d_S -covariance field yields results different from the d_E -covariance field (d_E being the Euclidean metric). In order to compare the d_S -covariance and d_E -covariance fields visually, one could in principle use dimension reduction methods; however the interpretation of projections of the d_S -covariance may be problematic, as discussed in Section 3.1. An alternative way to represent the d -covariance variations is to consider a single location of interest and plot the distances between the d -covariance at the location of interest, and the d -covariances at all other locations of the map. This produces 2D surfaces that reflect which parts of the country are more similar or dissimilar to the location of interest with respect to d -covariance. Figure A10 shows an example of these distance surface for the square-root and the Euclidean metric, where the distance between d -covariances has been computed using the d_S metric in both cases (averaged over the length of the sound), and the distances have been renormalized to the interval $[0, 1]$ to allow for fair comparison of the plots. The tuning parameters are $h = 1, k = 32$ nearest locations. Notice that the level curves are different. In particular, the level curve 0.6 for the square-root map goes down to Bristol, whereas it goes down to Dorset in the Euclidean metric map. The level curve 0.8 is also very different between the two maps. These differences can be attributed

suffolk: ipswich, uk

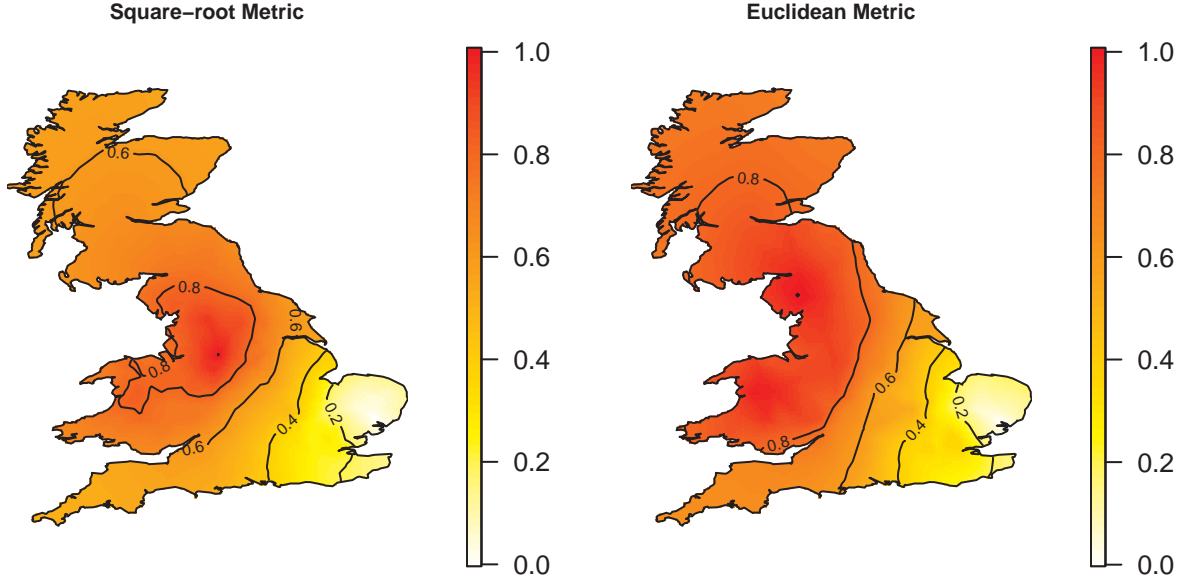


Figure A10: Left: color map with contours of the pairwise distances between the d_S -covariance at Ipswich (Suffolk), and the d_S -covariance at other locations. Right: same color map, but for the d_E -covariance. The tuning parameters are $h = 1, k = 32$ nearest locations. The scale of each map has been renormalized so that the value 1 is the maximal pairwise distance (under the metric d_S) in the d -covariance field, respectively for each metric.

to the swelling effect of the Euclidean metric (Arsigny et al. 2007).

References

- Arsigny, V., Fillard, P., Pennec, X. & Ayache, N. (2006), ‘Log-Euclidean metrics for fast and simple calculus on diffusion tensors’, *Magnetic resonance in medicine* **56**(2), 411–421.
- Arsigny, V., Fillard, P., Pennec, X. & Ayache, N. (2007), ‘Geometric means in a novel vector space structure on symmetric positive-definite matrices’, *SIAM Journal on Matrix Analysis and Applications* **29**(1), 328–347.
- Aston, J. A., Chiou, J.-M. & Evans, J. P. (2010), ‘Linguistic pitch analysis using functional principal component mixed effect models’, *Journal of the Royal Statistical Society: Series C (Applied Statistics)* **59**(2), 297–317.
- Axler, S. (2015), *Linear algebra done right*, 3rd ed. edn, Cham: Springer.

- Baíllo, A. & Grané, A. (2009), ‘Local linear regression for functional predictor and scalar response’, *Journal of Multivariate Analysis* **100**(1), 102–111.
- Boj, E., Caballé, A., Delicado, P., Esteve, A. & Fortiana, J. (2016), ‘Global and local distance-based generalized linear models’, *Test* **25**(1), 170–195.
- Boj, E., Delicado, P. & Fortiana, J. (2010), ‘Distance-based local linear regression for functional predictors’, *Computational Statistics & Data Analysis* **54**(2), 429–437.
- Carmichael, O., Chen, J., Paul, D. & Peng, J. (2013), ‘Diffusion tensor smoothing through weighted karcher means’, *Electronic journal of statistics* **7**, 1913.
- Coleman, J., Aston, J. & Pigoli, D. (2015), Reconstructing the sounds of words from the past, in The Scottish Consortium for ICPHS 2015, ed., ‘Proceedings of the 18th International Congress of Phonetic Sciences’, the University of Glasgow, Glasgow, UK. Paper number 0296.
- Coleman, J., Baghai-Ravary, L., Pybus, J. & Grau, S. (2012), ‘Audio bnc: the audio edition of the spoken british national corpus’, *Phonetics Laboratory, University of Oxford*.
URL: <http://www.phon.ox.ac.uk/AudioBNC>
- Cooley, J. W. & Tukey, J. W. (1965), ‘An algorithm for the machine calculation of complex Fourier series.’, *Math. Comput.* **19**, 297–301.
- Delicado, P., Giraldo, R., Comas, C. & Mateu, J. (2010), ‘Statistics for spatial functional data: some recent contributions’, *Environmetrics* **21**(3-4), 224–239.
- Dryden, I. L., Koloydenko, A. & Zhou, D. (2009), ‘Non-Euclidean statistics for covariance matrices, with applications to diffusion tensor imaging’, *The Annals of Applied Statistics* **3**(3), 1102–1123.
- Erro, D., Sainz, I., Navas, E. & Hernáez, I. (2011), HNM-based MFCC+F0 extractor applied to statistical speech synthesis, in ‘ICASSP, IEEE International Conference on Acoustics, Speech and Signal Processing - Proceedings’, pp. 4728–4731.
- Erro, D., Sainz, I., Navas, E. & Hernaez, I. (2014), ‘Harmonics plus noise model based vocoder for statistical parametric speech synthesis’, *IEEE Journal on Selected Topics in Signal Processing* **8**(2), 184–194.
- Fan, J. & Gijbels, I. (1995), ‘Data-driven bandwidth selection in local polynomial fitting: variable bandwidth and spatial adaptation’, *Journal of the Royal Statistical Society. Series B (Methodological)* **57**, 371–394.
- Francis, W. N. (1959), ‘Some dialect isoglosses in england’, *American Speech* **34**(4), 243–250.
- Gold, B., Morgan, N. & Ellis, D. (2011), *Speech and Audio Signal processing: Processing and Perception of Speech and Music*, John Wiley & Sons.

- Gromenko, O., Kokoszka, P., Zhu, L. & Sojka, J. (2012), ‘Estimation and testing for spatially indexed curves with application to ionospheric and magnetic field trends’, *The Annals of Applied Statistics* **6**(2), 669–696.
- Hadjipantelis, P. Z., Aston, J. A. & Evans, J. P. (2012), ‘Characterizing fundamental frequency in mandarin: A functional principal component approach utilizing mixed effect models’, *The Journal of the Acoustical Society of America* **131**(6), 4651–4664.
- Hadjipantelis, P. Z., Aston, J. A., Müller, H.-G. & Evans, J. P. (2015), ‘Unifying amplitude and phase analysis: A compositional data approach to functional multivariate mixed-effects modeling of mandarin chinese’, *Journal of the American Statistical Association* **110**(510), 545–559.
- Kraus, D. & Panaretos, V. M. (2012), ‘Dispersion operators and resistant second-order functional data analysis’, *Biometrika* **99**(4), 568–603.
- Kretschmar, W. A. (1996), ‘Quantitative areal analysis of dialect features’, *Language Variation and Change* **8**(01), 13–39.
- Lehmann, C. (2004), ‘Data in linguistics’, *The Linguistic Review* **21**(3-4), 175–210.
- Menafoglio, A. & Petris, G. (2016), ‘Kriging for hilbert-space valued random fields: The operatorial point of view’, *Journal of Multivariate Analysis* **146**, 84–94.
- Nerbonne, J., Colen, R., Gooskens, C., Kleiweg, P. & Leinonen, T. (2011), ‘Gabmap-a web application for dialectology’, *Dialectologia: revista electrònica* pp. 65–89.
- Nerbonne, J. & Kretschmar, W. (2003), ‘Introducing computational techniques in dialectometry’, *Computers and the Humanities* **37**(3), 245–255.
- Petersen, A. & Müller, H.-G. (2016a), ‘Fréchet integration and adaptive metric selection for interpretable covariances of multivariate functional data’, *Biometrika* **103**(1), 103–120.
- Petersen, A. & Müller, H.-G. (2016b), ‘Fréchet Regression for Random Objects’, *ArXiv e-prints*.
- Pigoli, D., Aston, J. A., Dryden, I. L., Secchi, P. et al. (2014), ‘Distances and inference for covariance operators’, *Biometrika* **101**(2), 409–422.
- R Core Team (2016), *R: A Language and Environment for Statistical Computing*, R Foundation for Statistical Computing, Vienna, Austria.
URL: <https://www.R-project.org/>
- Sangalli, L. M., Ramsay, J. O. & Ramsay, T. O. (2013), ‘Spatial spline regression models’, *Journal of the Royal Statistical Society: Series B (Statistical Methodology)* **75**(4), 681–703.
- Srivastava, A., Wu, W., Kurtek, S., Klassen, E. & Marron, J. (2011), ‘Registration of functional data using fisher-rao metric’, *arXiv preprint arXiv:1103.3817*.

- The Functional Phylogenies Group (2012), ‘Phylogenetic inference for function-valued traits: speech sound evolution’, *Trends in Ecology & Evolution* **27**(3), 160–166.
- Tucker, J. D., Wu, W. & Srivastava, A. (2013), ‘Generative models for functional data using phase and amplitude separation’, *Computational Statistics & Data Analysis* **61**, 50–66.
- Upton, C. & Widdowson, J. D. A. (2013), *An Atlas of English Dialects: Region and Dialect*, Routledge.
- van der Loo, M. P. (2014), ‘The stringdist Package for Approximate String Matching’, *R Journal* **6**(1), 111–122.
- Wang, H., Marron, J. et al. (2007), ‘Object oriented data analysis: Sets of trees’, *The Annals of Statistics* **35**(5), 1849–1873.
- Wood, S. N., Bravington, M. V. & Hedley, S. L. (2008), ‘Soap film smoothing’, *Journal of the Royal Statistical Society: Series B (Statistical Methodology)* **70**(5), 931–955.
- Wu, W. & Srivastava, A. (2014), ‘Analysis of spike train data: Alignment and comparisons using the extended fisher-rao metric’, *Electronic Journal of Statistics* **8**(2), 1776–1785.
- Yuan, Y., Zhu, H., Lin, W. & Marron, J. S. (2012), ‘Local polynomial regression for symmetric positive definite matrices’, *Journal of the Royal Statistical Society: Series B (Statistical Methodology)* **74**(4), 697–719.